

LASER INDUCED IONIZATION OF ARGON

Kenneth G.H. Baldwin

September, 1979

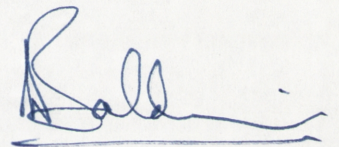
*a thesis submitted towards the degree of Master of
Science at the Australian National University*

Department of Engineering Physics,
Research School of Physical Sciences
Australian National University
Canberra, A.C.T.

(i)

STATEMENT

The experimental and theoretical investigations presented in this thesis are the original work of the author except where otherwise acknowledged. No part of this thesis has been submitted towards a degree or diploma in any other university or tertiary institution.



K.G.H. BALDWIN

September, 1979

ABSTRACT

A method of determining the laser intensity necessary for ionization of atomic states is described. The results of ionization of argon states I to V at 10^{-4} torr using a short (25 ps) pulse neodymium laser are presented. They agree tentatively with computer calculations of the Keldysh (1965) tunnelling model in the transition regime $\gamma \leq 1$. The electron energy spectra technique used further verifies the existence of the ponderomotive force.

ACKNOWLEDGEMENTS

I would like to thank my supervisor, Dr B.W. Boreham, for the proposal of this project and for his guidance during its preparation. I would also like to thank the members of the Laser Physics Laboratory for their assistance during the running of the experiment (particularly Dr G.B. Gillman) and for their many helpful discussions, especially with Dr B. Luther-Davies who also provided much practical assistance. The technical staff of the Laboratory were also very helpful during the experimental work, particularly Mr W. Hopkinson who assisted greatly in the running and improvement of the experimental apparatus. Finally, I would like to mention my gratitude to Dr L. Hughes and to Professor S. Kaneff, Head of the Department of Engineering Physics, whose earlier efforts to obtain support had enabled my undertaking of this project.

CONTENTS

CHAPTER I – INTRODUCTION	1
CHAPTER II – THEORY	
1. VALIDITY CRITERION	6
2. MULTIPHOTON IONIZATION	8
3. KELDYSH THEORY	10
4. RESONANCES, POLARIZATION AND FIELD STATISTICS	12
5. IONIZATION CALCULATIONS	14
6. PONDEROMOTIVE FORCE	18
CHAPTER III – EXPERIMENT	
1. SHORT PULSE LASER	26
2. LASER DIAGNOSTICS	29
3. BANDWIDTH LIMITING	31
4. LASER INTENSITY DISTRIBUTION	33
5. DETECTION CHAMBER	33
6. PRESSURE CONSIDERATIONS	39
CHAPTER IV – RESULTS	
1. INTRODUCTION	43
2. BACKGROUND TESTING	43
3. EXPERIMENTAL RESULTS	45
4. DISCUSSION	53
CHAPTER V – CONCLUSION	56
REFERENCES	58

LIST OF FIGURES

Table No.

2.1	Calculated ionization threshold intensities for helium and argon.	16
-----	--	----

Figure No.

2.1	Theoretical ionization threshold intensity.	17
2.2	Theoretical integrated electron energy spectra	24
3.1	Experimental layout	27
3.2	Short pulse laser	28
3.3	Two photon fluorescence monitor	30
3.4a	TPF pulse width display	32
3.4b	Integrated detector signal	32
3.5	Iso-intensity surfaces.	34
3.6	Volume enclosed by iso-intensity surfaces.	35
3.7	Test chamber detector arrangement	36
3.8	Multidirectional analyser configuration.	37
4.1	Sample electron energy contours.	46
4.2	Electron energy contours	48
4.3	Integrated electron energy spectra.	49
4.4	Sample electron energy spectra	51
4.5	Experimental and theoretical ionization threshold intensities.	52

CHAPTER I

INTRODUCTION

The advent of lasers in the early 1960's brought about an increased interest in ionization of gases by high frequency electromagnetic radiation, with previous work having been confined mainly to microwave ionization. Extensive experimental and theoretical work on laser induced ionization has been carried out and was the subject of review papers by a number of authors (Bakos 1974, Grey-Morgan 1975, Hughes 1975, Delone 1975, Lambropoulos 1976 and Stenholm 1979). The various mechanisms by which ionization due to high frequency electromagnetic radiation occurs has been the subject of considerable debate (particularly in the regime of strong electric fields) and as such is of fundamental physical interest.

The first rigorous treatment of laser induced ionization was made by Keldysh (1965) who demonstrated the inherently similar nature of the two major ionization processes proposed at that time. The first of these was multiphoton ionization for which the ionization probability is essentially determined by the probability of absorption of k photons (energy $\hbar\omega$) such that $k\hbar\omega \geq \chi$ (where χ is the ionization potential). This process has a characteristic power law dependence on the laser intensity (I) given by $W \propto I^k$, where W is the ionization probability and k is the minimum number of photons required for ionization. Keldysh showed that this process was valid in the weak electric field (low intensity) regime, but that as the laser intensity increased a transition occurred to a second process that operated in the strong field regime. The transition occurred when a quantity Keldysh defined as $\gamma \propto (\chi/I)^{1/2}$ was of order 1 (see II.1), with multiphoton effects occurring for $\gamma \gg 1$. The latter process, in the region $\gamma \ll 1$, was shown by Keldysh to resemble auto-ionization due to tunnelling in an alternating electric field. Keldysh stressed, however, that the two processes were not competing mechanisms but merely two limiting cases of the same ionization process.

The bulk of experimental and theoretical work carried out to date has been confined to the investigation of multiphoton ionization for two main reasons. Firstly, until recently, only low laser powers were available which restricted experiments to the weak field region ($\gamma \gg 1$). Secondly, the majority of theoretical calculations have used perturbational methods which break down outside the multiphoton regime once the perturbation due to the strong electric field becomes too large. As a consequence most experiments have aimed at verification of theoretical calculations by measuring the power law dependence and the total generalised ionization cross-section σ (from $W = \sigma I^k$).

The experimental technique used was almost universal and consisted of a laser beam focussed into a target chamber containing the test gas at pressures below 10^{-1} torr. Ions produced in the focal region were extracted by means of a static electric field and detected by a Faraday cup or similar arrangement. By changing the laser intensity slightly, the slope of a plot on a log-log scale of ion number versus intensity would reveal the power law dependence, provided that the percentage of atoms ionized in the focal region was small. Chin and Izenor (1970) pointed out that if a large percentage of atoms in the focal volume were ionized, then an increase in intensity would cause saturation of the ion signal due to depletion of the number of neutral atoms in the focal region. Any further intensity rise would increase the signal only as a result of the expansion of the focal volume within which all the atoms were ionized. This placed a further restriction on the laser intensity used to investigate multiphoton ionization since the intensity had to be sufficiently low in order to guarantee that only a small percentage of atoms in the focal volume were ionized.

Using this technique a number of experiments measured the power law dependence and ionization cross-section, mainly for rare gases and alkali elements (see for example Voronov and Delone 1966, Agostini *et al.* 1968, 1970). Many of these revealed power law dependences as would be expected from multiphoton perturbation theory, but some discovered exponents smaller than the number of photons required for ionization (e.g. Agostini *et al.* 1968). This was attributed to the presence of intermediate resonance levels with energies relative to the ground state equal to an integral number of photon energies. The finite lifetime of these levels enhanced the total ionization probability since the ionization process occurred in two steps: multiphoton excitation to an allowed intermediate atomic energy level followed by photoionization with the absorption of only a few more photons. The rate determining step in this case was the first process, and consequently a lower order power dependence of the ionization probability was observed. With increased laser intensities, Stark shifting of the intermediate resonance levels due to the strong electric field was predicted and observed in some cases (Delone and Delone 1969), although at high intensities the problems mentioned previously were again encountered.

Until recently, no observations were made of the electron/ion energy spectra since the particles were usually accelerated from the focal region by an externally applied electric field. Martin and Mandel (1976) and Hollis (1978), however, did observe electrons produced by intense laser radiation with energies well in excess of that expected due to photon absorption alone (a few $\text{eV} \sim \hbar\omega$). The explanation for such high energies (ranging from tens to hundreds of eV) was that electrons produced by ionization could be accelerated by a force due to the intensity gradient of the radiation field. First introduced by Hora (1969 a,b) as the 'ponderomotive force' to explain the observation of high velocity ions emitted from laser produced plasmas, the force accelerates charged particles down the electric field

gradient away from the high intensity region at the focal centre (see 11.6). Since it can be shown that the energy gained by the electron reflects the intensity distribution in the laser focal region, the measured electron energies could in certain circumstances be used to determine the intensity at which ionization occurred. However, because of inadequate monitoring of experimental parameters, no quantitative verification of the ponderomotive force model's relation to the electron energies was possible from either Martin and Mandel or Hollis's work.

Experiments by Boreham and Luther-Davies (1979) were aimed at determining quantitatively this relationship and to attempt to explain the electron energy spectra observed. High energy electrons were again detected (several hundred eV) for intensities up to 10^{16} W cm⁻² and the electron spectra indeed coincided with that expected from the ponderomotive force model. It was found that the low energy limit of the electron spectra was determined by the ionization threshold intensity at which electrons were first observed. The maximum detected electron energy (which is determined by the time and space history of the pulse in the focal region) was also observed to increase in proportion to the peak laser intensity in accordance with the ponderomotive force model. Since the laser intensity was large enough to cause saturation ionization of the focal volume then the number of electrons varied in proportion to the size of the ionized volume, in contrast to previous experiments where the intensity (and hence the ionized fraction) was deliberately kept low to avoid saturation. Debye coupling effects on the electrons which caused some of their energy to be given up to ion motion were also in good agreement with theoretical predictions.

A most important consequence of these experiments was the observation of the onset of ionization for helium I at an intensity corresponding approximately to that predicted by the Keldysh theory in the tunnelling limit (with $\gamma \sim 0.6$). This was also verified from the shape of the electron energy spectra (by the technique described in 11.6). The results encouraged speculation as to whether higher ionization states could be observed using the same technique at higher intensities. Previous experiments, which relied solely on plotting electron or ion yield as a function of laser intensity in order to determine the power law dependence of the ionization process, could not have been expected to reveal higher ionization states than the first. This was due to the high intensities required to ionize most second ionization electrons, which would result in saturation of the first ionization process within the focal volume. The signal from first ionization electrons would be much greater than from second ionization electrons, and the former would increase with the focal volume as the intensity increased. This would obscure the higher power law dependence (due to the higher ionization potential) of the second ionization electron yield, even assuming that the multiphoton limit applied at the intensities required for second (or higher) ionization states. In virtually all atoms suitable for such studies, the intensities required to observe second ionization would be within the tunnelling regime predicted by Keldysh and would thus not necessarily be expected to obey a multiphoton power law dependence even if this was observable.

By analysis of the electron energy spectra, however, higher ionization states could conceivably be observed. Electrons produced by second ionization (for example in helium) could be discriminated from first ionization electrons due to their greater energy, since they would be ionized at higher intensities and would thus experience greater acceleration from the steeper electric field gradient. With this in view, Boreham (1979c) carried out further experiments in helium using improved intensity measuring and electron detection apparatus. Helium was chosen because of the well separated first and second ionization states at 24.6 eV and 54.4 eV respectively (Kelly and Harrison, 1971) and because of the absence of higher ionization states which could confuse the observations. The results clearly indicated the presence of two separate groups of electron velocities corresponding to the first and second ionization states of helium. Calculations also showed that the ionization threshold intensities at which the two states were first observed corresponded approximately to the predictions of the Keldysh tunnelling model. However, the ionization states of helium fall just on the border of the tunnelling regime defined by Keldysh ($\gamma \sim 1$) and this, combined with the large experimental errors, meant that these results could not by themselves be considered a validation of the Keldysh theory.

The applicability of tunnelling versus multiphoton processes had already come under question following the work of Lompre *et al.* (1976) who had shown a strict multiphoton power law dependence for first ionization in rare gases. This, however, was done at laser intensities of $\sim 10^{15} \text{ W cm}^{-2}$ which for helium and neon gave a value for γ of $\sim 0.3 - 0.4$. Curiously, no focal region saturation effects were observed in direct contradiction to the work of Boreham and Luther-Davies (1979) and Boreham (1979c), since the laser intensity was more than sufficient to fully ionize the focal region. Lompre *et al.* (1977) made further measurements in rare gases, this time at much lower intensities ($\sim 10^{13} \text{ W cm}^{-2}$) at which saturation effects would not be present. Again a strict multiphoton power law relation was observed, but this time in the regime $\gamma \sim 2$. A similar experiment in xenon by Alimov and Delone (1976) at intensities $< 10^{13} \text{ W cm}^{-2}$ (giving $\gamma \sim 5$) also produced a multiphoton power law dependence which, as Alimov and Delone explain, would strictly only be expected for $\gamma \gg 1$. They point out however, that approximating the Keldysh ionization probability by a power law over the narrow range of intensity variation used in the experiments yielded a value of k^* indistinguishable from the number of photons k required for ionization (within the error limits achieved by the experiment.) Thus not even for first ionization is the conventional measurement of power law dependence useful for the determination of ionization processes in the $\gamma \sim 1$ regime.

As a result it was decided to investigate the nature of the ionization process by determining the threshold intensity at which the onset of ionization occurred, and to test this against the thresholds predicted by both the tunnelling and multiphoton limits in the strong field regime. This required a test gas with a number of ionization states accessible in the intensity range available ($10^{14} - 10^{17} \text{ W cm}^{-2}$) covering the regime $\gamma = 1.0 - 0.1$. Argon, with outer shell ionization states at 15.8, 27.6, 40.7, 58.8, 75.0, 91.0, 124.3 and

143.4 eV (Kelly and Harrison, 1971) satisfied this criterion and was the gas employed in this experiment.

The theoretical ionization threshold conditions were calculated for each ionization state by a computer program and checked by hand calculations as described in II.5. Chapter II also outlines the theory behind the Keldysh model, as well as the ponderomotive force mechanism which was used to identify the onset of the various ionization states. The experimental set up was similar to that employed by Boreham (1979c) and is documented in detail in Chapter III. This chapter also explains the criterion used to determine the test gas number density so as to ensure unambiguous interpretation of the integrated electron spectra obtained in the experiment. The results of the experiment are documented in Chapter IV along with a discussion of their interpretation and significance. Finally, a summary of the conclusions derived from this experiment and suggestions for further investigation of laser induced ionization processes using strong electric fields are given in Chapter V.

CHAPTER II

THEORY

1. VALIDITY CRITERION

The theory of Keldysh (1965) was the first attempt to identify the processes occurring in laser induced ionization in a strong radiation field and to define their dependence on the basic parameters characterizing both the atom (ionization potential χ) and the field (angular frequency ω and strength E). Using a quasiclassical analysis of the removal of an electron from a rectangular potential well of depth $\chi \gg \hbar\omega$, Keldysh discovered that laser induced ionization proceeded according to a general solution that had two limiting cases. The first of these was a tunnelling process that occurred when the electron emerged through the potential barrier in a time short compared with the reciprocal of the field frequency. The second was a multiphoton process that required the simultaneous absorption of a number of photons in a series of virtual transitions with lifetimes governed by the energy–time uncertainty relation. The criterion defining which of these two limiting cases occurred was given by the adiabatic limit of the tunnelling of an electron through a potential barrier under the action of a constant external electric field.

Consider an electron in a potential well (depth χ) to which can be assigned a velocity of the order of

$$v = \sqrt{\frac{2\chi}{m_e}} \dots\dots\dots 2.1$$

where m_e is the electron mass. The size of the region where the ground state electron can reach the continuum is defined by

$$l = \frac{\chi}{eE} \dots\dots\dots 2.2$$

where e is the charge on the electron. Over this distance, the field provides enough energy to overcome the potential well depth. An estimate of the tunnelling frequency ω_t can thus be obtained using equations 2.1 and 2.2 in

$$\begin{aligned} \omega_t &= \frac{v}{2l} \\ &= \frac{eE}{\sqrt{2m_e\chi}} \dots\dots\dots 2.3 \end{aligned}$$

This is merely the reciprocal of the tunnelling time, and if this is short compared to one period of the alternating electric field, then tunnelling of the electron through the potential barrier can occur. This criterion is expressed by the adiabatic parameter

$$\begin{aligned} \gamma &= \frac{\omega}{\omega_t} \\ &= \frac{\omega \sqrt{2m_e \chi}}{eE} \dots\dots\dots 2.4 \end{aligned}$$

where $\gamma \ll 1$ in the tunnelling limit, and $\gamma \gg 1$ when multiphoton processes occur. Examination of equation 2.4 shows that tunnelling occurs for low frequency, strong field radiation, while multiphoton ionization occurs in the high frequency, weak field limit. For neodymium lasers ($\omega = 1.77 \times 10^{15} \text{ rad s}^{-1}$) and ionization potentials of $\sim 10 - 20 \text{ eV}$ (for commonly used gases such as Ar, Ne and Xe), the transitional field strength is $2 - 3 \times 10^8 \text{ V cm}^{-1}$ ($\equiv 0.5 - 1.0 \times 10^{14} \text{ W cm}^{-2}$). As was noted in Chapter I, practical limitations such as saturation have previously restricted experimental investigation of laser induced ionization to intensities below this level, and corroboration of theoretical predictions was thus only possible in the multiphoton regime ($\gamma \gg 1$).

Limitations also occur on the validity of theoretical work on multiphoton processes since the majority of calculations have been carried out using perturbation theory. The applicability of such methods relies on the perturbation due to the external light field being small compared to the field of the atomic system (E_{at}). It is difficult to define an exact criterion for the validity of perturbational methods because of the complex nature of the perturbation of the atomic spectrum by the light field. However, following Delone (1975), the upper limit of the light field intensity is defined by requiring that the oscillation energy of the electron in the field be much less than the energy of the free electron removed from the atom (i.e. $\leq \hbar\omega$).

This criterion can be written as

$$\frac{E}{E_{at}} \ll (k)^{-3/2} \dots\dots\dots 2.5$$

where E_{at} is the field intensity in the orbit of the ground state of hydrogen ($5 \times 10^9 \text{ V cm}^{-1}$) and $k = \chi / \hbar\omega$. Using a typical value for the number of photons k required for ionization of ~ 10 , then from equation 2.5, the field strength for perturbation theory to be valid is $\ll 10^8 \text{ V cm}^{-1}$ ($\ll 10^{13} \text{ W cm}^{-2}$). As laser induced ionization is multiphoton in nature up to field intensities slightly higher than this, there is a region ($\sim 5 \times 10^7 - 3 \times 10^8 \text{ V cm}^{-1}$) for which perturbation theory is not applicable.

In comparison, Keldysh's quasiclassical model is formulated to allow description of ionization in the presence of a strong light field. In the multiphoton limit of the Keldysh theory, ionization occurs slowly in comparison with atomic times at optical and infra-red frequencies (since $\omega_t \ll \omega \ll \omega_{at} = \chi/\hbar$). This essentially requires that

$$\frac{E}{E_{at}} \ll 1 \dots\dots\dots 2.6$$

thus indicating that Keldysh's quasiclassical approximation is applicable for the multiphoton regime well into the region of high field strength ($E \ll 5 \times 10^9 \text{ V cm}^{-1}$ or $I \ll 3 \times 10^{16} \text{ W cm}^{-2}$).

2. MULTIPHOTON IONIZATION

Since the field strengths used in this experiment ($> 5 \times 10^8 \text{ V cm}^{-1}$) were well in excess of those in which perturbational multiphoton treatments are valid, ($\ll 10^8 \text{ V cm}^{-1}$), only a brief summary of these methods will be given. Multiphoton ionization is essentially a series of transitions between virtual states (resonances with intermediate atomic states are not considered here) which have lifetimes determined not by relaxation but by the energy-time uncertainty relation. (An approximation to the virtual state lifetime Δt is given by $\hbar\omega \times \Delta t \sim \hbar$ which gives $\Delta t \sim 10^{-15} \text{ s}$.) The virtual state lifetimes are consequently very small and hence in order that a transition to a higher state be made with a non-negligible probability, very large photon fluxes obtainable only from high power lasers are necessary.

Using time-dependent perturbation theory formalism, consider the Hamiltonian H of the system (atom and radiation field) divided into the interaction Hamiltonian V and the Hamiltonian H_0 of the separate unperturbed systems of atom and field,

$$H = H_0 + V \dots\dots\dots 2.7$$

Since the dimensions of the atomic system are small compared with the wavelength of the laser light ($\sim 1 \mu\text{m}$), then the atom can be considered to be acted upon by a classical and monochromatic field through the ordinary dipole interaction

$$V = -e \underline{r} \cdot \underline{E} \cos\omega t \dots\dots\dots 2.8$$

Using the eigenfunctions of the unperturbed system n_i , the transition amplitude from the ground state g to the ionized final state f is proportional to the product of the k individual transition amplitudes

$$V_{gf} \propto \sum_{n_{k-1}} \dots \sum_{n_1} V_{gn_1} V_{n_1 n_2} \dots V_{n_{k-1} f} \dots \quad 2.9$$

The ionization probability is thus

$$W_{gf} \propto |E^k|^2 |r_{afa_g}|^2 \dots \quad 2.10$$

where

$$r_{afa_g} \propto \sum_{a_{k-1}} \dots \sum_{a_1} r_{a_g a_1} r_{a_1 a_2} \dots r_{a_{k-1} a_f}$$

and a_i are the eigenstates of the unperturbed atomic system.

Hence, since $I \propto E^2$

$$W_{gf} = \sigma_{gf} I^k \dots \quad 2.11$$

where σ_{gf} is the generalized total ionization cross-section. This is the origin of the power law dependence of the ionization probability on the laser intensity for multiphoton processes.

The calculation of ionization probability is dependent on being able to evaluate the transition matrix element r_{afa_g} . This presents two difficulties (Delone 1975), the first being the usual one of construction of a wave function of the electron in a complex atom. The second arises because of the occurrence of virtual transitions which necessitates an infinite summation in the calculation of the compound transition matrix elements. The various summation methods (for example, Gold and Bebb, 1965), characterize the different techniques for evaluating the generalized ionization cross-section and hence in determining the ionization probability for multiphoton ionization. It should also be mentioned in passing that other methods, such as the momentum translation approximation (see Reiss 1970, Choudhury 1973a,b) which were initially proposed as alternative non-perturbative theories, have since been shown to be merely rearrangements of perturbation theory and have been discarded.

3. KELDYSH THEORY

The quasiclassical theory of Keldysh (1965) considered the general case of the ionization of an atom in a strong (linearly polarized) light field using the model problem of removal of an electron from a rectangular potential well. Keldysh used perturbation theory to calculate the transition probability from a bound state to a final state that, unlike the usual perturbation theory which used a stationary final state, took into account the main effect of the electric field – the acceleration of the free electron in the oscillating field to an average energy (see II.6)

$$\xi_{\text{osc}} = \frac{e^2 E^2}{4m\omega^2} \dots\dots\dots 2.12$$

The matrix elements of the transitions between the bound states were taken into account only in the lower orders of the perturbation theory since they are proportional to eEa_0 (a_0 being the Bohr radius). Keldysh was able to show that the transition matrix elements taken into account in the continuous spectrum were proportional to $eEa_0 (\chi/\hbar\omega)^{1/2}$ (where $\chi/\hbar\omega \sim k \gtrsim 10$).

As a result of these calculations, Keldysh obtained a general formula for the ionization probability in which the field strength E appears only via the adiabaticity parameter γ . The solution is

$$W = A\omega \left(\frac{\chi}{\hbar\omega}\right)^{3/2} \left(\frac{\gamma}{(1+\gamma^2)^{1/2}}\right)^{5/2} S\left(\gamma, \frac{\chi^*}{\hbar\omega}\right) \\ \times \exp \left\{ -\frac{2\chi^*}{\hbar\omega} \left[\sinh^{-1} \gamma - \gamma \frac{(1+\gamma^2)^{1/2}}{1+2\gamma^2} \right] \right\} \dots\dots\dots 2.13$$

where χ^* is the effective ionization potential (with the added energy of the electron oscillating in the light field)

$$\chi^* = \chi + \frac{e^2 E^2}{4m\omega^2} \dots\dots\dots 2.14$$

and $S(\gamma, \chi^*/\hbar\omega)$ is a relatively slowly varying function of the frequency and field strength in comparison with the exponential. A is a numerical coefficient of order unity.

In the tunnelling limit ($\gamma \ll 1$), the following expression was obtained for the ionization probability

$$W(\gamma \ll 1) = \frac{\sqrt{6\pi}}{4} \frac{\chi}{\hbar} \left(\frac{eE\hbar}{m^{1/2}\chi^{3/2}} \right)^{1/2} \times \exp \left\{ -\frac{4}{3} \frac{\sqrt{2m}\chi^{3/2}}{eE\hbar} \left(1 - \frac{m\omega^2\chi}{5e^2E^2} \right) \right\} \dots\dots\dots 2.15a$$

$$= \frac{1}{4} \left(\frac{6\pi\sqrt{2}\omega}{\hbar} \right)^{1/2} \left(\frac{\chi}{\gamma} \right)^{1/2} \times \exp \left\{ -\frac{4}{3} \frac{\chi}{\hbar\omega} \gamma \left(1 - \frac{\gamma^2}{10} \right) \right\} \dots\dots\dots 2.15b$$

The ionization probability is highly dependent on the exponential function, which in turn is strongly dependent on the electric field strength E. Any variation in the pre-exponential factor thus has only a minor effect when calculating the field strength necessary to achieve a certain ionization probability.

One of the restrictions of the formula 2.15 above is that it does not take into account the effect of the Coulomb interaction on the final state, which is important due to the long range of electrostatic forces. This would be expected to increase the ionization probability since the electron would essentially not have to overcome the entire energy depth of the potential well. However, inclusion of the Coulomb interaction results only in a change in the power of E in the pre-exponential expression without altering the exponential itself, and thus the form of the correction is not as crucial as might first appear. Using a crude quasiclassical analysis (verified also by Nikishov and Ritus, 1967), the correction factor (apart from a numerical coefficient) was given by Keldysh as $\chi \gamma / [\hbar\omega(1 + \gamma^2)]^{1/2}$ and is included in the equation 2.13. Thus 2.15 becomes

$$W(\gamma \ll 1) = \frac{1}{4\hbar\omega} \left(\frac{6\pi\sqrt{2}\omega}{\hbar} \right)^{1/2} \chi^{3/2} \gamma^{1/2} (1 + \gamma^2)^{-1/2} \times \exp \left\{ -\frac{4}{3} \frac{\chi}{\hbar\omega} \gamma \left(1 - \frac{\gamma^2}{10} \right) \right\} \dots\dots\dots 2.16$$

This increases the ionization probability by a factor ~ 10 for the experimental gases considered here (near their ionization threshold where $W \sim 1$) but does not significantly influence their threshold intensity. The formula 2.16 also agrees with the exact expression derived by Perelemov *et al.* (1966) for the hydrogen atom in the ground state subject to linearly polarized light if the undefined numerical coefficient is given a value of $\frac{16}{\pi} (2)^{3/4}$.

The ionization probability corrected for the Coulomb interaction with the final state (expression 2.13) should be applicable to a description of the ionization of any atom

or ion. This is due to the fact that the ionization probability is essentially determined by the action of the field on the final state of the free electron and not on the ground state of the atom (as was noted previously). Hence, the use of another ground state wave function will not alter the ionization probability appreciably since the ground state interactions affect only the pre-exponential factor.

In the other limiting case ($\gamma \gg 1$) corresponding to multiphoton ionization, the general Keldysh formula (2.13) for the ionization probability has been approximated by Raizer (1965) in a form useful for numerical evaluation:

$$W = B\omega N^{3/2} \left(\frac{e^2 E^2}{8m\omega^2\chi} \right)^N \dots\dots\dots 2.17$$

where N is the number of quanta necessary to exceed the effective ionization potential χ^* , and B is a numerical coefficient of order unity. Once again, the pre-exponential factor is of little importance since in estimating the threshold ionization intensity ($I \propto E^2$), any variation in B yields only a $B^{1/N}$ variation in the intensity. The power law dependence of the ionization probability on the laser intensity is again evident, although the dependence on the field frequency is somewhat different from previous perturbational calculations. The important difference however, is that the exponential includes the effect of the final state energy of the electron via the oscillation energy term in the effective ionization potential.

4. RESONANCES, POLARIZATION AND FIELD STATISTICS

The analysis so far has considered only the simplest ionization process and has not taken into account the effect of intermediate atomic resonances, light polarization and the statistical nature of the light source. The first effect has already been mentioned as lowering the power law dependence in the case of weak field multiphoton ionization. However, its effect in the strong field limit is not readily apparent, since the changing field strength during the pulse may alter the resonance levels due to the Stark effect, bring some states into temporary resonance and cause smearing of the upper levels with the continuum.

While Keldysh in his treatment included the effect of resonant states, the technique could not effectively be applied to high intensity fields for the reasons above. However, experimental evidence (Lompre *et al.* 1976, 1977) showed that although the laser frequency was tuned through a range that included resonances with atomic states, no resonant enhancement of the number of ions was observed. Their laser pulse length was, however, much shorter (~ 30 ps) than those commonly employed in such experiments, and further theoretical work by McLean and Swain (1978) indicated that at such short pulse durations, no resonant effects should be observed. The reason for this was that the pulse duration was much shorter than the lifetime of the atomic state ($< 10^{-7}$ s) and hence the

presence of the state did not increase the probability of absorption of an additional photon. Because of this and the difficulties involved in predicting the effect of strong fields on resonances, the influence of intermediate atomic states was not considered in the calculation of ionization probabilities for this experiment (in which the pulse duration was ~ 25 ps).

To this point only the effect of linearly polarized light has been considered in the ionization process, but it is obvious that since the final state is in the continuum and has available all possible angular momentum states, then light of any polarization can lead to ionization. The total ionization probability will, however, be dependent on the polarization, since the final state is a superposition of partial waves each with well defined angular momentum and each with different possible photon absorption pathways (channels) leading to the final partial wave (see Lambropoulos, 1976). The contribution of each partial wave is determined by the number of channels available via intermediate states which satisfy angular momentum conservation with the final partial wave, and also by the strength of the transition matrix elements. For low order ionization ($k < 4$) circular polarization gives a higher ionization probability (despite the fewer pathways available) due to the strength of the matrix elements. However, for higher order processes ($k > 4$), linear polarization yields higher probabilities as a result of the large number of channels available. Linearly polarized light was used in this experiment and in the calculations which follow.

Finally, the effect of light field statistics on the ionization probability must be mentioned. Since multiphoton ionization is essentially a coincidence measurement of the probability of a photon being absorbed by an electron in a virtual state, then the probability of a k photon process occurring is a measure of the k th order correlation function of the light field. For a monochromatic and coherent field the correlation function is given by (Mandel and Wolf, 1965)

$$C_{\text{COH}} \propto \bar{I}^k \dots\dots\dots 2.18$$

and this is the case for a mode-locked bandwidth limited laser pulse (as used in this experiment — see III.3) where \bar{I} is the average intensity. For a multiple longitudinal mode, Q-switched laser, however, the output approximates that of a thermal light source, the auto-correlation function for which is

$$C_{\text{th}} \propto K! \bar{I}^k \dots\dots\dots 2.19$$

Thus ionization by a multimode Q-switched laser is $K!$ more effective than for a mode-locked laser of the same mean intensity. Experimental evidence (Lecompte *et al.* 1974,

1975) has shown that for an 11 photon process in xenon, this ratio was $10^{6.9 \pm .3} \sim 11!$ despite the fact that the 100 mode laser used could not be considered an ideal thermal source. Indeed, the statistical properties of the laser were used by Arslanbekov *et al.* (1977) to determine the multiphoton nature of processes by measuring the above ratio for a 5 photon process in sodium (with $\gamma \gg 1$) and an 11 photon process in xenon (with $\gamma \sim 5$). Their results showed the ratio to be $10^{2.04 \pm .2} \sim 5!$ in the first case and $10^{5 \pm 1} \ll 11!$ in the second, thus indicating some departure from the multiphoton nature of the process as γ approached the region where multiphoton ionization could no longer be expected to be valid.

5. IONIZATION CALCULATIONS

Although the Keldysh theory of ionization in the regime of strong light fields was devised at an early stage in the investigation of laser induced ionization, it has yet to be superseded either in its general description of ionization processes or in its calculation of ionization probability for specific cases. The simplifying use of short (~ 25 ps), mode-locked, linearly polarized laser pulses in this experiment facilitated comparison of calculations using the Keldysh model and overcame the problem of resonances with intermediate states.

The aim of the calculations was to determine the laser intensity necessary to completely ionize a given level (1st, 2nd, 3rd etc.) at a given region in space assuming that the laser pulse shape was Gaussian in time. It was also assumed that the temporal pulse shape was the same over the entire focal region (see III.4: the laser pulse intensity varied from a maximum at the centre of the focal region (the central laser intensity) to regions of lesser intensity mapped as the concentric iso-intensity regions shown in fig. 3.5). Consequently, if the laser temporal height (the peak intensity) corresponded to the ionization threshold intensity for a given state at a certain point on an iso-intensity contour, then all atoms on and inside that contour would be ionized to that state. Owing to the strong dependence of the ionization probability on the field intensity, a rapid fall-off in the ionization probability would be expected just outside this contour even though the intensity may have decreased only slightly. As a consequence, most electrons produced will have originated inside the region defined by the outermost contour to have attained the ionization threshold intensity.

The ionization threshold intensity is defined as the peak intensity I_{TH} of a Gaussian pulse (half width $\tau = 25$ ps)

$$I = I_{TH} e^{-\left(\frac{2t}{\tau}\right)^2 \ln 2} \dots\dots\dots 2.20$$

which satisfies the condition

$$\int_{-\infty}^{\infty} W(I) dt = 1 \dots\dots\dots 2.21$$

The form for the ionization probability used in this experiment was the Coulomb corrected Keldysh tunnelling formula (2.16) which when evaluated gave

$$W = 2.294 \times 10^{19} \left(\frac{X}{I}\right)^{7/4} \left(1 + \frac{X}{2.114 \times 10^{-13} I}\right)^{-1/2} \\ \times \exp \left\{ -2.4885 \times 10^6 \left(\frac{X^3}{I}\right)^{1/2} \left(1 - 4.730 \times 10^{11} \frac{X}{I}\right) \right\} \dots\dots\dots 2.22$$

where X is in eV and I in $W \text{ cm}^{-2}$. For each ionization state the intensity required to achieve condition 2.21 was calculated for a square pulse of length 25 ps, and this intensity was used as an estimate for the peak intensity of the more difficult case of a Gaussian pulse (half-width 25 ps). The hand calculation and integration were then performed iteratively until condition 2.21 was also achieved for the Gaussian pulse. The results thus obtained for the (pulse peak) ionization threshold intensity differed by less than 0.3% from later computer code calculations.

The computer code was developed by Boreham (1979b) to perform the same calculation for the uncorrected Keldysh tunnelling formula and was later modified by the author to account for the Coulomb correction. The integration was performed using Simpson's rule with the integration limits being the e^{-2} points of the Gaussian pulse. Since the formula 2.22 is a strong function of the intensity, by far the major contribution to the integrated ionization probability came from the region at the pulse peak. As a consequence, most electrons were ionized in the small time interval (± 2 ps) around the pulse peak, and further calculations using the e^{-4} points as the integration limits made a negligible contribution to the total ionization probability. The larger the ionization potential used, the greater was the probability variation with intensity and hence the greater was the contribution from the pulse peak.

The results of the computer code calculations are tabulated in Table 2.1 and are shown graphically in fig. 2.1, where ionization threshold intensity is plotted against ionization potential. The second and third rows in Table 2.1 give the ionization thresholds for the uncorrected and Coulomb corrected Keldysh tunnelling formulas, with the exception of argon I for which the formula breaks down at an ionization potential ~ 16 eV. Extrapolation of the curve gives an ionization threshold for ArI of slightly less than $10^{14} W \text{ cm}^{-2}$. This is further confirmed in the calculation of the ionization probability for a CO_2 laser

ION	He I	He II	Ar I	Ar II	Ar III	Ar IV	Ar V	Ar VI	Ar VII	Ar VIII
1. IONIZATION POTENTIAL (eV)	24.59	54.42	15.76	27.63	40.74	58.81	75.0	91.0	124.3	143.4
2. UNCORRECTED KELDysh FORMULA (W cm ⁻²)	4.64 x 10 ¹⁴	4.74 x 10 ¹⁵	~ 10 ¹⁴	6.58 x 10 ¹⁴	2.06 x 10 ¹⁵	5.93 x 10 ¹⁵	1.20 x 10 ¹⁶	2.09 x 10 ¹⁶	5.15 x 10 ¹⁶	7.77 x 10 ¹⁶
3. COULOMB CORRECTED KELDysh FORMULA (W cm ⁻²)	3.29 x 10 ¹⁴	3.40 x 10 ¹⁵	~ 10 ¹⁴	4.67 x 10 ¹⁴	1.47 x 10 ¹⁵	4.26 x 10 ¹⁵	8.63 x 10 ¹⁵	1.51 x 10 ¹⁶	3.73 x 10 ¹⁶	5.63 x 10 ¹⁶
4. CO ₂ LASER (W cm ⁻²)	3.50 x 10 ¹⁴	3.44 x 10 ¹⁵	9.72 x 10 ¹³	4.89 x 10 ¹⁴	1.50 x 10 ¹⁵	4.31 x 10 ¹⁵	8.69 x 10 ¹⁵	1.52 x 10 ¹⁶	3.73 x 10 ¹⁶	5.64 x 10 ¹⁶
5. $\tau + 10\%$ (W cm ⁻²)	3.25 x 10 ¹⁴	3.37 x 10 ¹⁵	~ 10 ¹⁴	4.61 x 10 ¹⁴	1.45 x 10 ¹⁵	4.22 x 10 ¹⁵	8.54 x 10 ¹⁵	1.50 x 10 ¹⁶	3.69 x 10 ¹⁶	5.57 x 10 ¹⁶
6. $\tau - 10\%$ (W cm ⁻²)	3.34 x 10 ¹⁴	3.45 x 10 ¹⁵	8.13 x 10 ¹³	4.73 x 10 ¹⁴	1.48 x 10 ¹⁵	4.32 x 10 ¹⁵	8.74 x 10 ¹⁵	1.53 x 10 ¹⁶	3.77 x 10 ¹⁶	5.70 x 10 ¹⁶
7. $\gamma(z)$	0.59	0.28	~ 0.9	0.53	0.36	0.26	0.20	0.17	0.13	0.11
8. RAIZER FORMULA (W cm ⁻²)	3.56 x 10 ¹⁴	9.21 x 10 ¹⁴	1.91 x 10 ¹⁴	4.14 x 10 ¹⁴	6.62 x 10 ¹⁴	1.00 x 10 ¹⁵	1.31 x 10 ¹⁵	1.62 x 10 ¹⁵	2.25 x 10 ¹⁵	2.61 x 10 ¹⁵

Table 2.1. CALCULATED IONIZATION THRESHOLD INTENSITIES FOR HELIUM AND ARGON

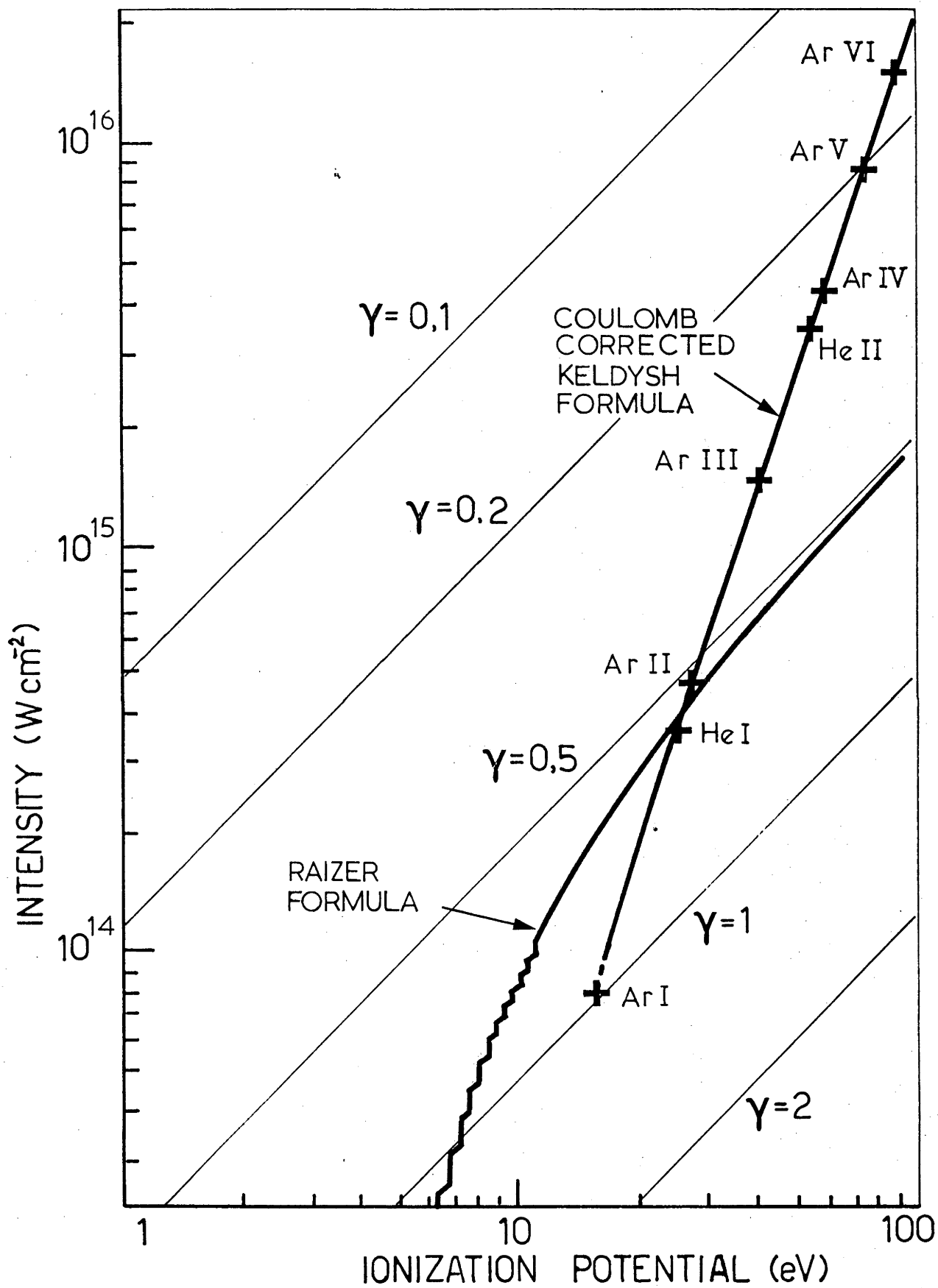


fig.2.1: THEORETICAL IONIZATION THRESHOLD INTENSITIES

with a frequency ω of 1.78×10^{14} rad s⁻¹ (10.6 μ m wavelength) – exactly once tenth that for a neodymium laser. As can be seen from equation 2.16, since $\gamma \propto \omega$ the ionization probability is essentially frequency independent, apart from the γ^2 terms which are negligible if $\gamma \ll 1$ (which it is, due to the lower frequency, by a factor of > 10). The lower value of γ is important here since the tunnelling formula now has a solution for $\chi \leq 16$ eV, and this gives an ionization threshold of 9.72×10^{13} W cm⁻² for argon I thus confirming the previous estimate. In fact, as can be seen from Table 2.1, the only deviation of neodymium thresholds from CO₂ thresholds occurs in the region (for neodymium) where γ approaches 1 (see row 7) i.e. in the regime for which the tunnelling formula ceases to be valid.

Also shown in Table 2.1 is the effect of variation in the laser pulse duration τ on the ionization intensity threshold. For $\pm 10\%$ variations in the pulse length, only a $\mp 1\%$ alteration occurred in the threshold intensity, with smaller variations occurring for higher ionization potentials. Again, the small effect on threshold intensities is due to the strong dependence of ionization probability on intensity, with only a small increase in peak intensity necessary to offset a large decrease in pulse length. Another indication that the argon I ionization threshold is less than 10^{14} W cm⁻² is given by the $\tau - 10\%$ pulse whose shorter length enables the probability integral to attain a value of 1 at a peak intensity of 8.13×10^{13} W cm⁻².

For comparison with the tunnelling limit of the Keldysh formula, the multiphoton ionization threshold intensities as given by the Raizer approximation (equation 2.17) are shown in row 8. These calculations were carried out manually due to the behaviour of the exponential N, which incremented in discrete amounts as the oscillation energy increased with intensity. This caused the discontinuities in the Raizer formula shown in fig. 2.1. As can be seen the discontinuities become almost negligible for ionization potentials approaching those used in experimental materials ($\chi > 10$ eV). It may finally be noted that the multiphoton and tunnelling formulas give approximately similar ionization thresholds in the transition region between the two regimes corresponding to $\gamma \sim 1$.

6. PONDEROMOTIVE FORCE

The acceleration of electrons within the beam was due to the ponderomotive force given by

$$f_{NL} = -\frac{e^2}{4m\omega^2} \nabla E_s^2 \dots\dots\dots 2.23$$

where e and m are the charge and mass of the electron, ω the field frequency and E_s the amplitude of the oscillating electric field. The force arises due to the large electric field gradient produced by the laser which accelerates electrons down the gradient away from the

laser central intensity peak. It was originally proposed by Hora (1969a,b, 1971) to explain fast ion production in laser produced plasmas, but was already known from previous theoretical work (see for example Landau and Lifshitz, 1960).

Following Chen (1974a,b) the equation of motion governing the electron behaviour is

$$m \frac{d\mathbf{v}}{dt} = -e [\mathbf{E}(\mathbf{r}) + \frac{1}{c} \mathbf{v} \times \mathbf{B}(\mathbf{r})] \dots\dots\dots 2.24$$

Assuming an oscillating electric field

$$\mathbf{E}(\mathbf{r}) = \mathbf{E}_s(\mathbf{r}) \cos \omega t \dots\dots\dots 2.25$$

and thus
$$\mathbf{B}(\mathbf{r}) = -\frac{c}{\omega} \nabla \times \mathbf{E}_s \sin \omega t \dots\dots\dots 2.26$$

from Maxwell's equations. To first order (neglecting the $\mathbf{v} \times \mathbf{B}$ term), at the initial position \mathbf{r}_0

$$m \frac{d\mathbf{v}_1}{dt} = -e \mathbf{E}(\mathbf{r}_0) \dots\dots\dots 2.27$$

which causes the electron to oscillate in the \mathbf{E} direction. Expanding $\mathbf{E}(\mathbf{r})$ about the initial position gives

$$\mathbf{E}(\mathbf{r}) \sim \mathbf{E}(\mathbf{r}_0) + \delta \mathbf{r} \cdot \nabla \mathbf{E} \dots\dots\dots 2.28$$

Integrating 2.27 twice gives

$$\mathbf{v}_1 = \frac{-e}{m\omega} \mathbf{E}_s(\mathbf{r}_0) \sin \omega t \dots\dots\dots 2.29$$

$$\delta \mathbf{r} = \frac{e}{m\omega^2} \mathbf{E}_s(\mathbf{r}_0) \cos \omega t \dots\dots\dots 2.30$$

Substituting the first order parts of 2.25 to 2.30 into 2.24 gives the second order part of the equation of motion

$$\begin{aligned}
 m \frac{dv_2}{dt} &= -e[\delta \underline{r} \cdot \underline{\nabla} E(\underline{r}_0) + \frac{1}{c} \underline{v}_1 \times \underline{B}(\underline{r}_0)] \\
 &= -e\left[\left(\frac{e}{m\omega^2} \underline{E}_S \cos \omega t \cdot \underline{\nabla}\right) \underline{E}_S \cos \omega t + \right. \\
 &\quad \left. \frac{1}{c} \left(\frac{-e}{m\omega} \underline{E}_S \sin \omega t \times \frac{-c}{\omega} \underline{\nabla} \times \underline{E}_S \sin \omega t\right)\right] \\
 &= \frac{-e^2}{m\omega} \left[(\underline{E}_S \cdot \underline{\nabla}) \underline{E}_S \cos^2 \omega t + \underline{E}_S \times (\underline{\nabla} \times \underline{E}_S) \sin^2 \omega t \right] \dots \text{.2.31}
 \end{aligned}$$

Averaging over time gives

$$\begin{aligned}
 m \left\langle \frac{dv_2}{dt} \right\rangle &= \frac{-e^2}{2m\omega^2} [\underline{E}_S \cdot \underline{\nabla} \underline{E}_S + \underline{E}_S \times \underline{\nabla} \times \underline{E}_S] \\
 &= \frac{-e^2}{4m\omega^2} \underline{\nabla} \underline{E}_S^2 \\
 &= \underline{f}_{NL} \dots \dots \dots \text{.2.32}
 \end{aligned}$$

Integrating 2.32 over the electric field gradient gives an energy

$$\begin{aligned}
 \xi_{KIN} &= \int_{(E_S)}^{(0)} \underline{f}_{NL} \cdot \underline{dr} \\
 &= \frac{e^2 |\underline{E}_S|^2}{4m\omega^2} \dots \dots \dots \text{.2.33}
 \end{aligned}$$

which is the same as the time averaged oscillation energy obtained by substituting 2.29 into

$$\xi_{OSC} = \frac{1}{2} m |\underline{v}_1|^2 \dots \dots \dots \text{.2.34}$$

Since $|\underline{E}_S|^2 = 7.54 \times 10^2 I \text{ V}^2 \text{ cm}^{-2} \dots \dots \dots \text{.2.35}$

(Lorrain and Corson, 1970) where I is in W cm⁻², rewriting 2.33 gives

$$\xi_{OSC} \sim 10^{-13} I \text{ J} \dots \dots \dots \text{.2.36}$$

This implies that the energy gained by an electron accelerated from the beam is proportional to the laser intensity at the electron's point of origin. It assumes that the laser intensity remains unchanged during the acceleration of the electron from the beam and the criterion for this condition is defined by two limiting cases.

Following Hollis (1978), consider the energy gained by an electron originating at a distance R from the beam axis (assuming axial symmetry). This is given by

$$\begin{aligned} \xi_{KIN} &= \int_{-\infty}^{\infty} \int_R^{\infty} f_{NL}(r(t), t) dr dt \\ &= \int_{-\infty}^{\infty} \int_R^{\infty} \frac{e^2}{4m\omega^2} \frac{\partial}{\partial r} (E_s(r(t)), t)^2 dr dt \dots\dots\dots 2.37 \end{aligned}$$

The radial and temporal dependences of the non-linear force are separable only in the following two approximations:

(i) The low intensity limit: In this case the electron is considered not to have moved at all during the pulse because of the low pulse intensity (and hence slow acceleration due to the ponderomotive force). Instead the electron is given an impulse

$$\begin{aligned} P &= \int_{-\infty}^{\infty} \int_R^{\infty} \delta_r(R) f_{NL}(r, t) dt dr \\ &= \int_{-\infty}^{\infty} f_{NL}(R, t) dt \dots\dots\dots 2.38 \end{aligned}$$

where $\delta_r(R)$ is the Dirac delta function. The maximum impulse will occur at the point of steepest slope in the radial intensity profile. For a Gaussian profile this occurs at $r_M = r_0(2)^{1/2}$ where r_0 is the half e^{-1} width. At this point

$$f_{NL}(r_M) = \frac{-e^2 E_s^2}{4m\omega^2} \left(\frac{-\sqrt{2}}{r_0} \exp^{-1/2} \right) \dots\dots\dots 2.39$$

and hence for a Gaussian pulse with half e^{-1} width T, using 2.38 and 2.39 gives

$$\begin{aligned} P_{MAX} &= \frac{e^2 E_s^2}{2\sqrt{2} m\omega^2 r_0} \exp^{-1/2} \int_{-\infty}^{\infty} e^{-t^2/T^2} dt \\ &= \left(\frac{\pi}{2} \right)^{1/2} \frac{e^2 E_s^2}{2m\omega^2} \frac{T}{r_0} \exp^{-1/2} \dots\dots\dots 2.40 \end{aligned}$$

This gives a maximum electron energy of

$$\begin{aligned}\xi_{\text{KIN}}^{\text{MAX}} &= p^2 / 2m \\ &\sim 2 \times 10^{-11} \left(\frac{IT}{r_0}\right)^2 \text{ eV} \dots\dots\dots 2.41\end{aligned}$$

where I is in W cm^{-2} , r_0 in cm and T is in seconds.

(ii) The high intensity limit: In this case the electron is considered to be swept out of the focal region in a time short compared with the pulse length due to the high pulse intensity. This eliminates the temporal dependence of the maximum possible electron energy since this will occur at the peak of the pulse. Thus (as before),

$$\begin{aligned}\xi_{\text{KIN}}^{\text{MAX}} &= \int_{-\infty}^{\infty} \int_R^{\infty} \delta_t(o) f_{\text{NL}}(r, t) dr dt \\ &= \int_R^{\infty} \frac{e^2}{4m\omega^2} \frac{\partial}{\partial r} (\nabla E_s^2(r)) dr \\ &= \frac{e^2 E_s^2}{4m\omega^2} \\ &\sim 10^{-13} I \text{ eV} \dots\dots\dots 2.42\end{aligned}$$

where I is the peak laser intensity in W cm^{-2} .

The transition between these two regimes would be expected to occur when the time of flight of the electron through the focal region approximates the pulse duration, i.e.

$$V_e \sim \frac{r_0}{T} \dots\dots\dots 2.43a$$

Using $r_0 \sim 6 \mu\text{m}$ and $T \sim 15 \text{ ps}$ this gives

$$V_e \sim 4 \times 10^7 \text{ cm/sec} \dots\dots\dots 2.43b$$

Thus, equating the maximum electron energies from the two regimes (2.41 and 2.42) we have

$$\begin{aligned}10^{-13} I &\sim 2 \times 10^{-11} \frac{I^2 T^2}{r_0^2} \\ \text{i.e. } I &\sim 4.7 \times 10^{-3} V_e^2 \\ &\sim 8 \times 10^{12} \text{ W cm}^{-2} \dots\dots\dots 2.44\end{aligned}$$

This corresponds to an electron energy of ~ 1 eV and hence electrons with $\xi_{KIN} \gg 1$ eV can be considered to have their energy governed by equation 2.42. As the peak intensities involved in this experiment were in the range 3×10^{14} W cm $^{-2}$ to 8×10^{16} W cm $^{-2}$ most of the electrons produced would be accelerated by the ponderomotive force in the high intensity limit.

The consequence of equation 2.42 is that a study of the electron energy spectra for varying laser intensities provides a useful diagnostic for the onset of ionization states. Consider the theoretical integrated electron energy spectra shown in fig. 2.2 for increasing laser intensities I_1 to I_5 where the number of electrons N_e (arbitrary units) greater than a given energy is plotted against that energy (eV). Initially (at low intensities) only the first ionization state is accessible for $I^1 < I < I_3$ (where I^1 is the ionization threshold intensity for the first ionization state). Inside the iso-intensity contour defined by I^1 all atoms will be singly ionized and consequently the minimum possible energy for a first ionization electron will be $10^{-13} I^1$ eV. This is reflected by the steep shoulder in the integrated electron spectra starting at around 14 eV, indicating a first ionization threshold intensity of around 1.4×10^{14} W cm $^{-2}$. For intensities less than this no first ionization will be observed and consequently no electrons of energy $\lesssim 14$ eV will be detected (hence the plateau below 14 eV). Electrons may achieve energies greater than 14 eV as for peak intensities greater than threshold, most atoms are ionized before the pulse peak. Consequently, if the electrons are not immediately ejected, those produced before the peak will experience a stronger accelerating field than if the pulse peaked at their threshold intensity. However, in the high intensity limit, the spectrum should fall off fairly rapidly after the shoulder in the plateau region.

Once $I > I^{II} > I_2$ second ionization electrons are accessible and these will be ejected from the beam with energies corresponding to $10^{-13} I^{II}$ eV. This produces the shoulder at ~ 80 eV indicating a second ionization threshold intensity of $\sim 8 \times 10^{14}$ W cm $^{-2}$. The plateau between the two shoulders shows that no electrons can be produced in the intensity range between the two ionization thresholds. Similarly a third ionization state is accessible above a threshold intensity of $\sim 4 \times 10^{15}$ W cm $^{-2}$.

An alternative means of identifying the various ionization states may be obtained by plotting the number of electrons detected (N_e) using a given retarding potential versus the laser intensity. From fig. 2.2 it would be expected that a bunching of such electron energy contours would occur at each ionization threshold intensity. For example, a plot of the 20 – 80 eV contours would show a grouping at an intensity I^{II} (between I_2 and I_3). This would indicate that the accessible electron energy had jumped from < 20 eV to > 80 eV due to the onset of the second ionization state. The bunching of electron energy contours at various intensities can thus be employed as a semi-independent means of checking the threshold ionization intensities obtained from the integrated electron spectra.

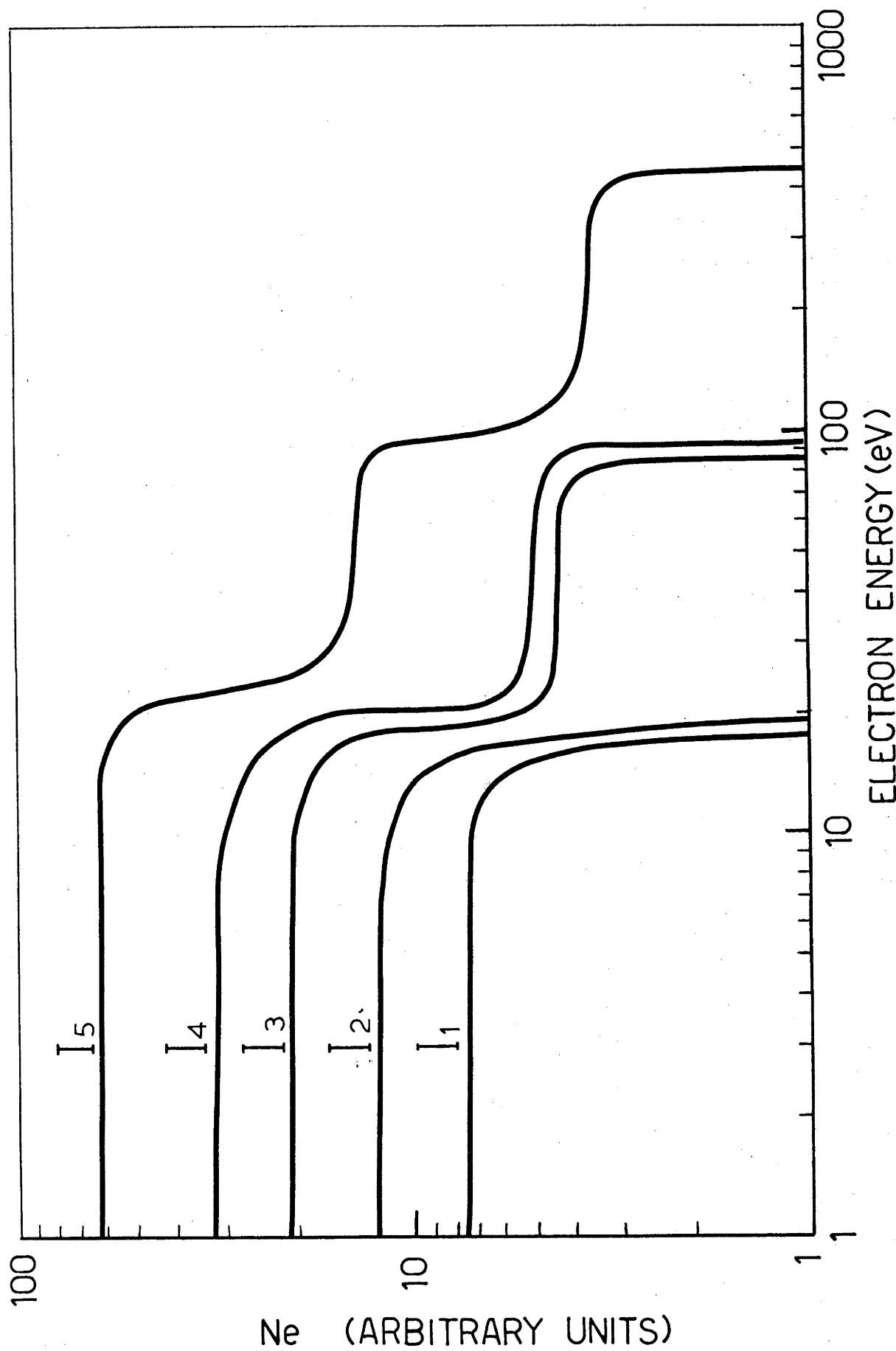


Fig. 2.2: THEORETICAL INTEGRATED ELECTRON ENERGY SPECTRA

This novel method of determining ionization threshold intensities could thus be expected to provide more information than a simple plot of electron yield versus laser intensity since the latter tends to lose the higher ionization states in the much larger detection signal due to first ionization.

CHAPTER III

EXPERIMENT

In order to investigate the validity of the Keldysh theory the experiment shown in fig. 3.1 was used as developed by Hollis (1976, 1978) and later expanded by Boreham *et al.* (1978, 1979). A single mode locked pulse was fired from the short pulse laser (SPL) into a test chamber filled to 10^{-4} torr with argon. The pulse was focussed within the test section, the electrons produced were collected by a detector, and the signal amplified, integrated and displayed on an oscilloscope. A retarding potential was applied to the detector to enable an integrated energy spectrum of the ionized electrons to be measured for various values of the peak laser intensity.

1. SHORT PULSE LASER

The neodymium short pulse laser system is illustrated schematically in fig. 3.2. The Nd:Yag laser oscillator (MLO) was passively mode locked using Kodak 9740 dye. It produced a train of pulses at a wavelength of $1.064 \mu\text{m}$ with energies up to 0.5 mJ and durations for 80% of pulses of between 18 and 36 ps (with a mean of 25 ps — Luther-Davies 1977). The first group of vertically polarized pulses passed through Pockels cell 1 (PC1) and was reflected by a Glan Taylor Prism (P1) which passed only horizontally polarised light. The reflected light was focussed to trigger a laser triggered spark gap which then applied a $\frac{1}{2}$ wave voltage to PC1. This selected a single pulse from later in the train which had its plane of polarization rotated to the horizontal, thereby allowing only that pulse to be passed by the polarizer. The beam profile was shaped by two apertures A1 and A2, the first of which diffracted the Gaussian output beam from the oscillator into an Airy diffraction pattern in the far field. The second truncated that pattern at its first zero producing a beam of finite diameter that would not suffer diffraction due to truncation at the edge of the laser amplifier rods. Such diffraction fringes would cause ripples on the laser output beam which when passed through the laser amplifier rods could self-focus (due to the refractive index non-linearity of the glass) and damage the amplifier rods. Further damage due to high frequency spatial modulations on the laser profile were prevented by a spatial filter (SF) and a vacuum spatial filter (VSF) which kept the incremental value of the beam break-up integral low (~ 1.1 at 40 GW). The lens forming part of the spatial filter essentially determined the beam expansion angle. The further two Pockels cells (allowing the pulse to be switched through via the delay lines) were designed to limit amplified spontaneous emission and to improve the main pulse-to-prepulse contrast ratio. The beam was amplified by

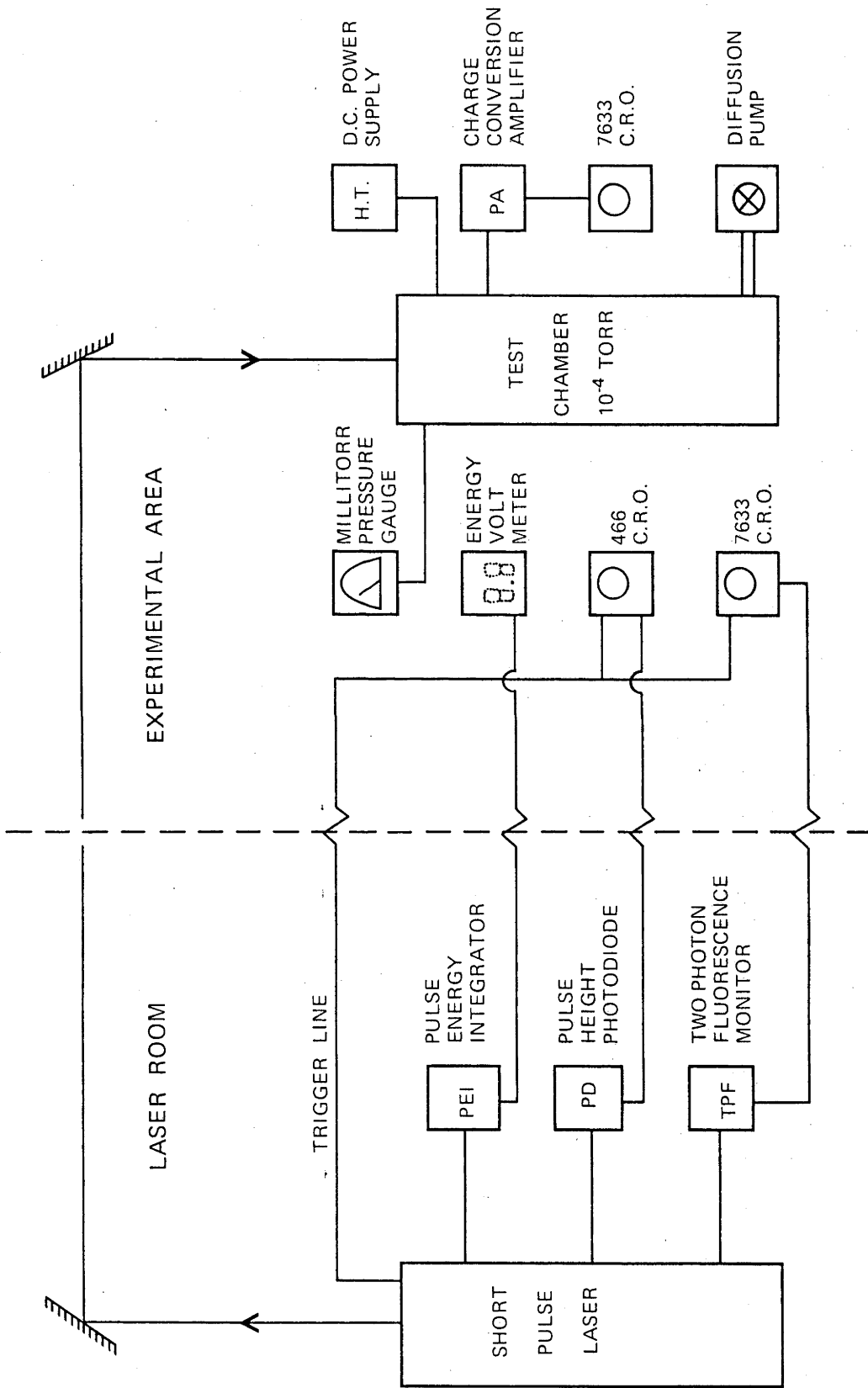


fig. 3,1: EXPERIMENTAL LAYOUT

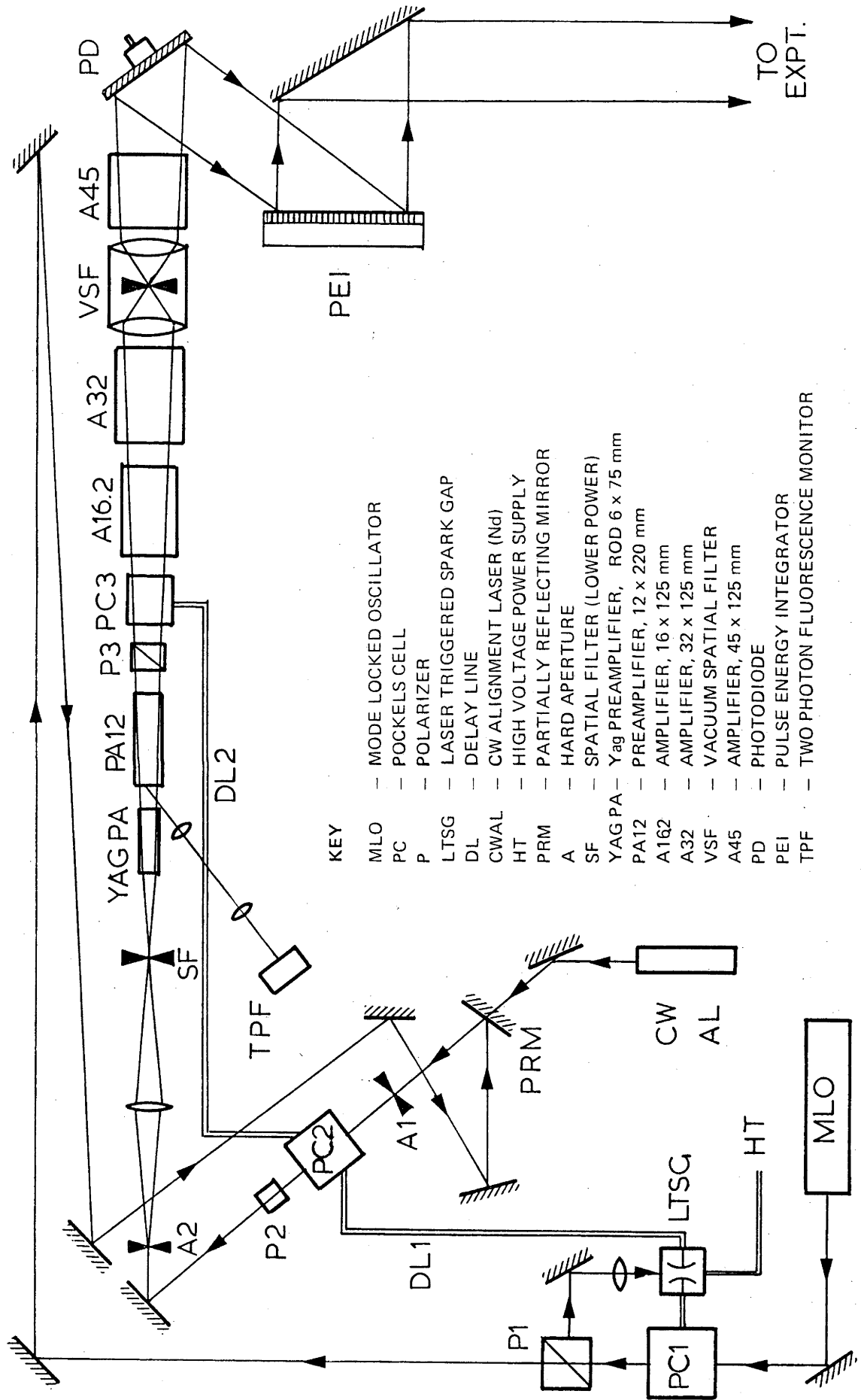


fig. 3.2: SHORT PULSE LASER

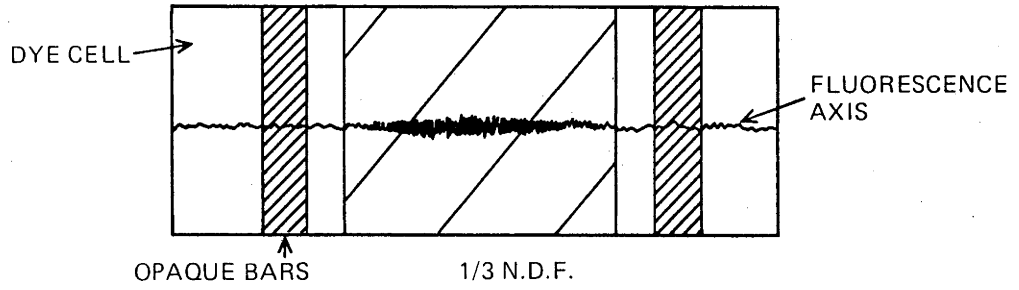
a series of Nd:Yag (Yag PA) and Nd:glass amplifiers (PA12, A16.2, A32, A45) used in various combinations to produce a final laser pulse with a peak power of 72 gigawatts (1.8 joules in 25ps).

2. LASER DIAGNOSTICS

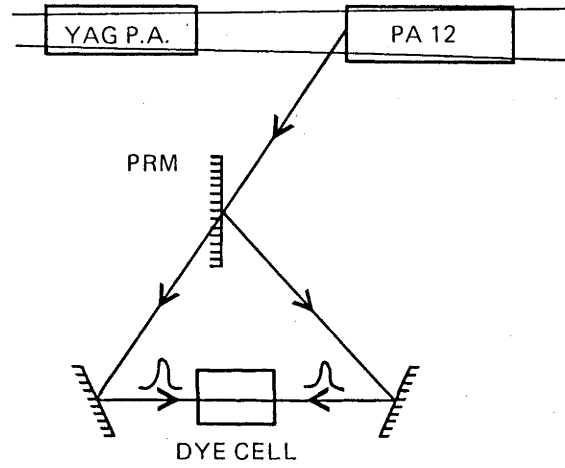
(i) Energy monitoring: Two methods were employed: (a) the laser pulse height was measured by displaying the output from a vacuum photodiode on a Tektronix 466 storage oscilloscope; and (b) the output pulse energy was integrated and displayed on a digital voltmeter. The latter was calibrated at $90 \pm 3 \text{ mJ/volt}$ at the beginning of the experiment, and was the primary energy diagnostic used. The laser pulse height was used as a check since some spurious pick-up of flashlamp light from the A45 amplifier registered on the energy voltmeter. It was also used to ensure that only one pulse was allowed through the pulse switch-out system since double pulses were readily visible on the pulse height monitor.

(ii) Pulse width monitoring: A two photon fluorescence (TPF) monitor (Bradley and New, 1974) was used to measure the laser temporal pulse width, and the method is outlined in fig. 3.3. As shown in fig. 3.3b, a small part of the beam was reflected off the front end of the PA12 amplifier and split in two by the partially reflecting mirror (PRM). The two beams produced were reflected again so that they met head-on inside the dye cell as shown. A 25 ps laser pulse travelling at the speed of light has spatial pulse length of about 5 mm in the dye and when the beams overlapped in the middle of the dye cell they created a region of increased fluorescence of about this length.

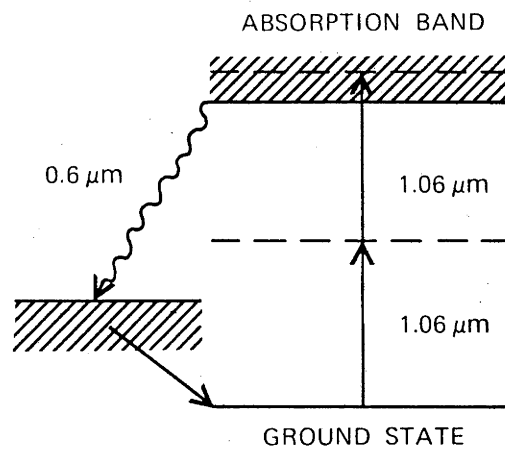
The fluorescent dye used in this monitor (Rhodamine 6G) required the simultaneous absorption of two photons at the laser wavelength to reach the absorption band (fig. 3.3c). Fluorescent decay to an intermediate energy level resulted in the emission of a visible $0.6 \mu\text{m}$ photon, the lifetime of the decay process being long compared with the laser pulse duration. As a consequence, the passage of the pulse produced a visible fluorescence axis in the dye (fig. 3.3a). At the point where the pulses overlap in time the peak intensity of the fluorescence should be three times that of the background region because of the power law dependence and autocorrelation effects (assuming that the pulse was bandwidth limited – see III.3). A neutral density filter was placed over the region of overlap with a transmission factor of $1/3$, and either side of this was a clear space followed by an



(a)



(b)



(c)

fig. 3.3: TWO PHOTON FLUORESCENCE MONITOR

opaque bar. A TV camera monitored the dye cell in this configuration and one line of the TV image was selected for display on a Tektronix 7633 oscilloscope.

Starting from the left hand opaque bar, the C.R.O. display showed a region of zero intensity, then a region of unity intensity followed by a Gaussian shaped region with the same peak intensity. This was again followed by a uniform unity intensity region and then by another zero intensity region. A typical such C.R.O. trace is shown in fig. 3.4a, the slight asymmetry being due to distortion in the TV camera scan. The half width of the Gaussian spatial pulse gave the half width of the laser pulse with a calibration of 18ps/division when the unity regions were separated by 6 divisions. By this method the pulse length of the laser was measured to within 10% ($\pm 2-3$ ps).

3. BANDWIDTH LIMITING

As mentioned in II.4, in order that a comparison between the theoretical and experimental ionization rates can be made, the autocorrelation function of the laser pulse must be known. Lompre *et al.* (1977) point out that if the pulse is bandwidth limited, i.e. devoid of intensity and frequency modulation, then its correlation function is unity and hence a comparison is easier. However, this requires careful monitoring of each laser pulse in both time and frequency domains to ensure that the pulsewidth-linewidth product is in the range

$$0.45 < \Delta\nu \times \Delta t < 1 \dots\dots\dots 3.1$$

where 0.45 is the product for a perfectly bandwidth limited Gaussian pulse.

Lompre *et al.* employed a mode-locked Nd:glass laser and monitored the pulse length using a pico-second resolution streak camera, while simultaneously measuring the linewidth with a diffraction grating spectrograph. No such techniques were available in this experiment but several indications of bandwidth limiting were possible. Firstly, the Nd:Yag oscillator used in this experiment has inherently 'cleaner' characteristics than Nd:glass oscillators used in similar configurations (such as employed by Lompre *et al.* who found that their Nd:glass pulses were bandwidth limited). Secondly, the two photon fluorescence pulse monitor gave some indication of gross abnormalities in the auto correlation function of each pulse.

This occurred through observation of the symmetry and smoothness of the TPF pulse shape, and also from the ratio of the central TPF pulse height to that of the unobstructed intensity regions. This ratio should be 1:1 with the neutral density filters in place and assuming bandwidth limiting. The ratio is less if this is not the case, although small deviations from bandwidth limiting would not be observed by this method. Thus, by careful monitoring of the TPF pulse shape it could be ascertained that the pulses used were close to bandwidth limited.

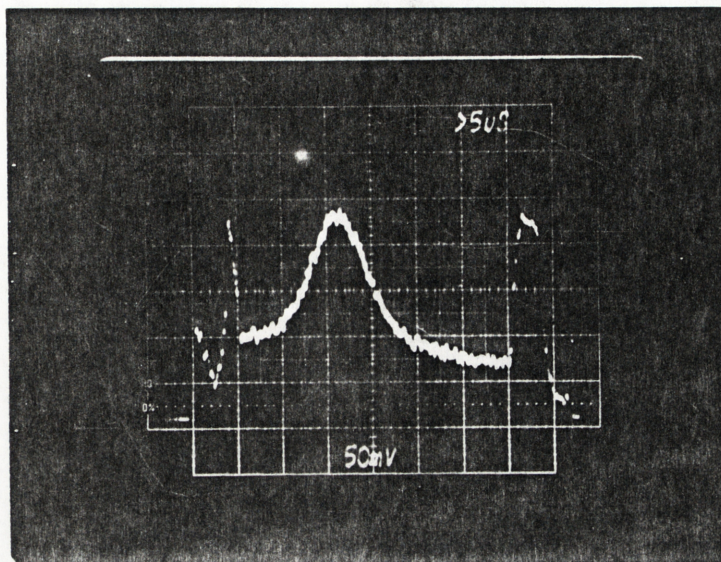


fig. 3,4a: TPF PULSE WIDTH DISPLAY

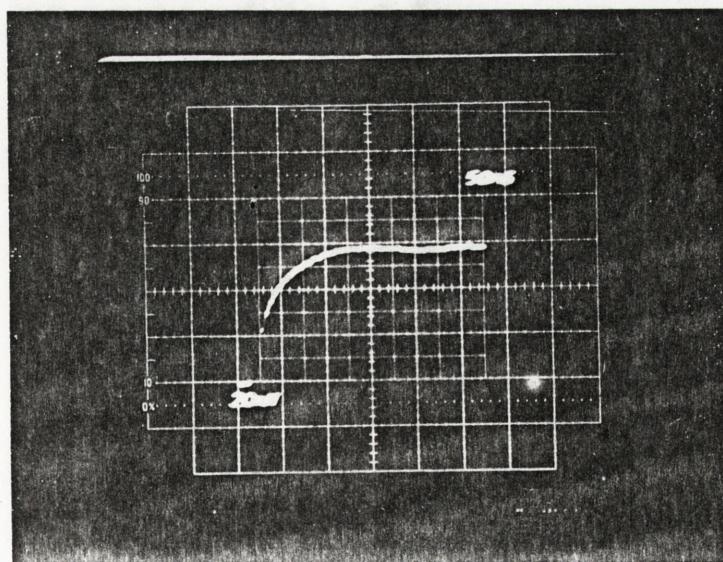


fig. 3,4b: INTEGRATED DETECTOR SIGNAL

4. LASER INTENSITY DISTRIBUTION

Having obtained the laser power from the integrated energy meter and the TPF monitor a knowledge of the energy distribution after focussing within the experimental chamber was necessary to determine the laser intensity at a given point within the focal volume. This had been measured in an earlier experiment (Boreham and Luther-Davies, 1979) and an intensity contour diagram is shown for the focal region in fig. 3.5. The iso-intensity contours are expressed as a fraction of the central intensity and were obtained by ablating an aluminium film from a glass substrate. In the focal plane the beam had an approximately Gaussian profile. The radial diameter of the intensity profile was $13 \pm 2 \mu\text{m}$ and this gave a central laser intensity of

$$I = \frac{E/\tau}{\frac{\pi}{4}(13 \times 10^{-4})^2} \text{ W cm}^{-2} \dots\dots\dots 3.2$$

where E is the laser energy in joules and τ the laser pulse half-width in seconds. Peak laser intensities of between 3×10^{14} and $4 \times 10^{16} \text{ W cm}^{-2}$ were obtained in the focal region. The volume enclosed by the various iso-intensity contours is shown in fig. 3.6 where the relative intensity is plotted against the volume relative to a standard volume $V^*(5 \times 10^{-8} \text{ cm}^3)$.

5. DETECTION CHAMBER

The detection chamber shown in fig. 3.7 was employed in the same configuration used by Boreham (1979a,c) and similar to that used by Hollis (1976, 1978) and Boreham *et al.* (1979). The chamber was modified slightly to improve the stability of the vacuum and to decrease the contamination due to diffusion pump oil. This was particularly important in view of the low ionization potential of diffusion pump oil on comparison to argon. The chamber was pumped to around 10^{-6} torr as measured by two Varian millitorr gauges (accurate to within 20%).

The laser beam was focussed using a 75 mm aperture $f = 1.5$ aspheric lens mounted immediately behind the entrance window. The laser alignment on the window was checked using the CW Nd:Yag laser (fig. 3.2) and verified by placing polaroid film in front of the window and ensuring that the laser burn pattern was centred correctly. Any electrons produced on the lens or window surfaces were shielded from the detector by beam skimming apertures.

The detector arrangement consisted of four separate detectors mounted perpendicular to the laser axis in a multidirectional configuration as shown in fig. 3.8.

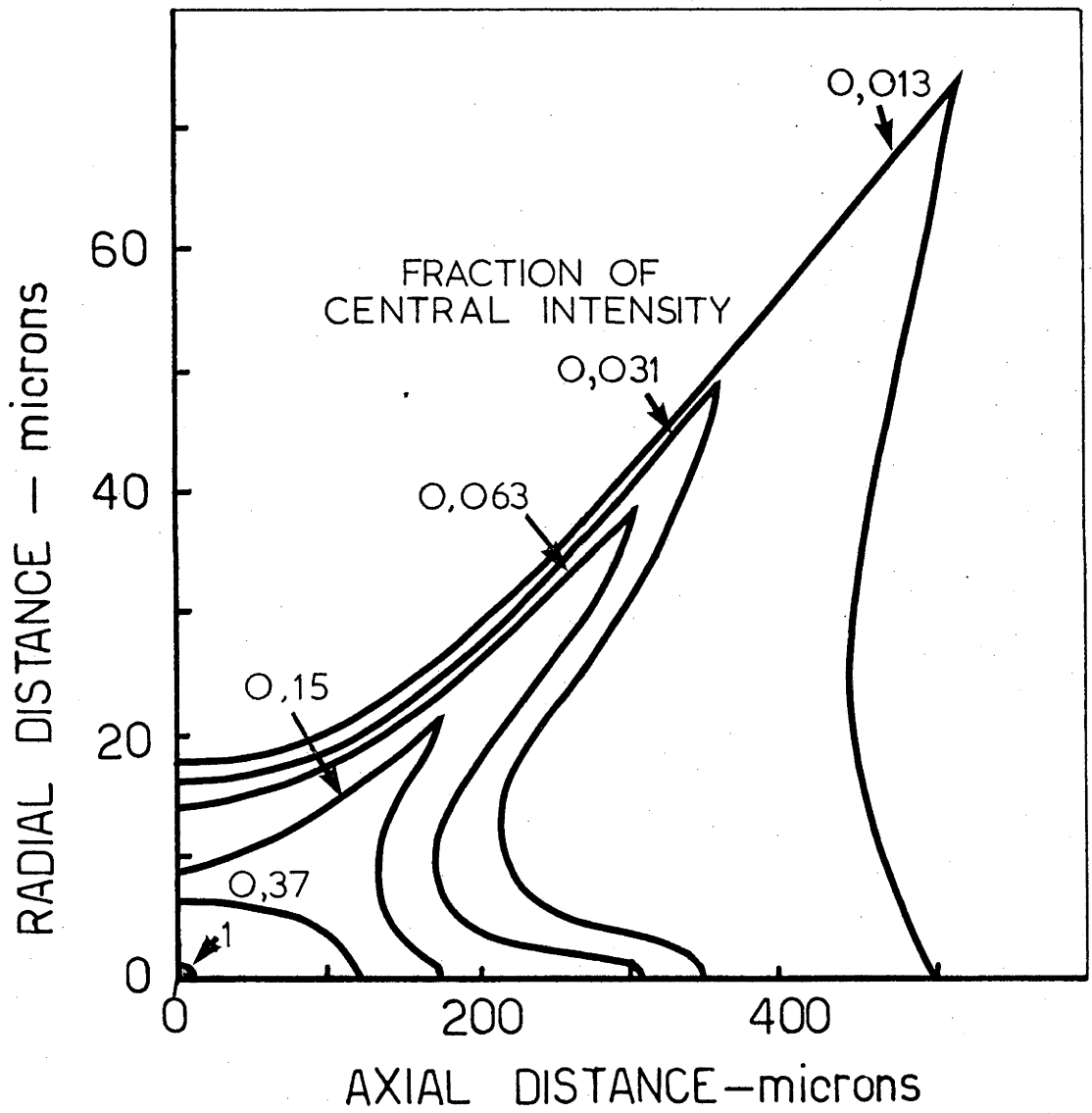


fig. 3,5: ISO-INTENSITY SURFACES

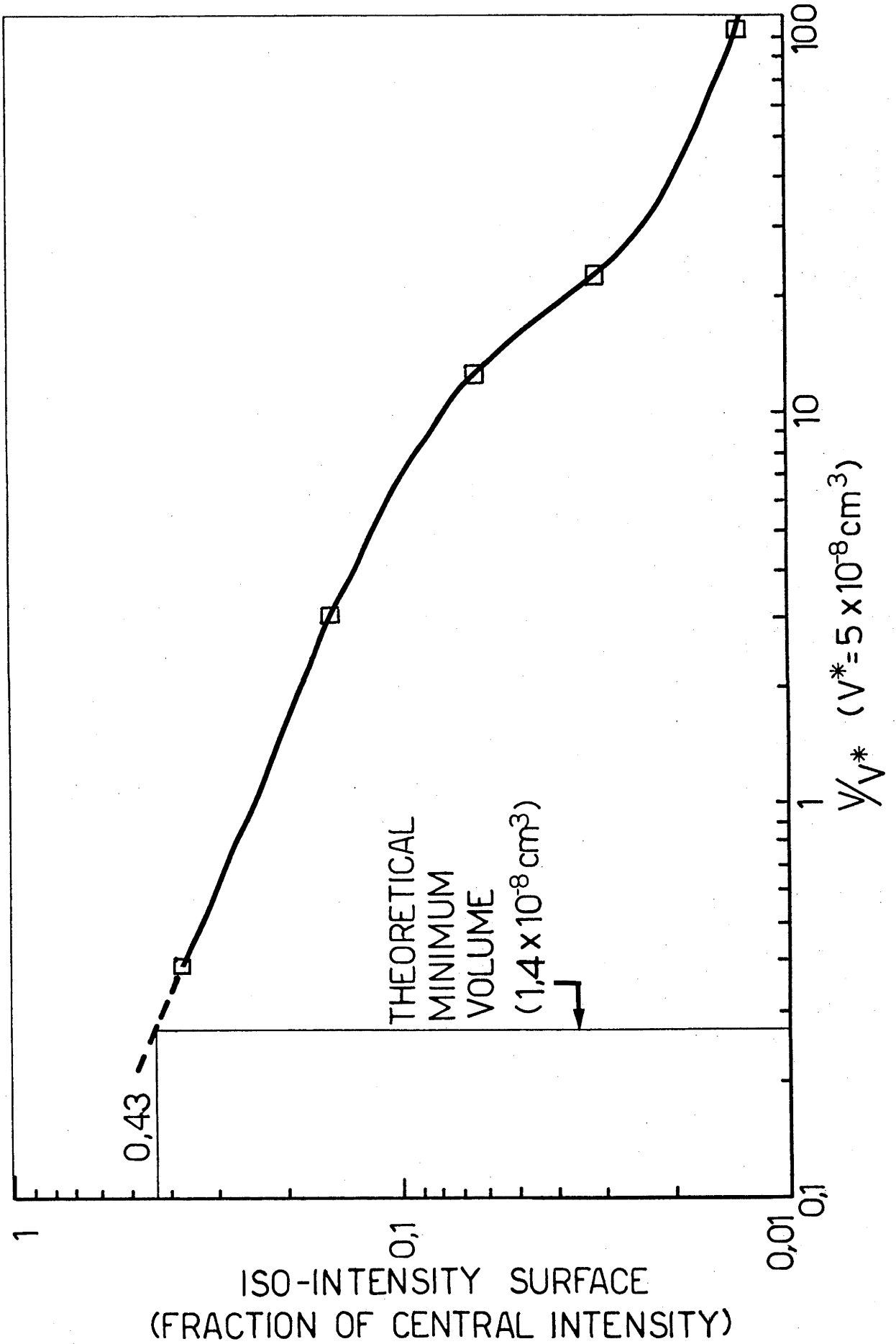


fig. 3,6: VOLUME ENCLOSED BY ISO-INTENSITY SURFACES

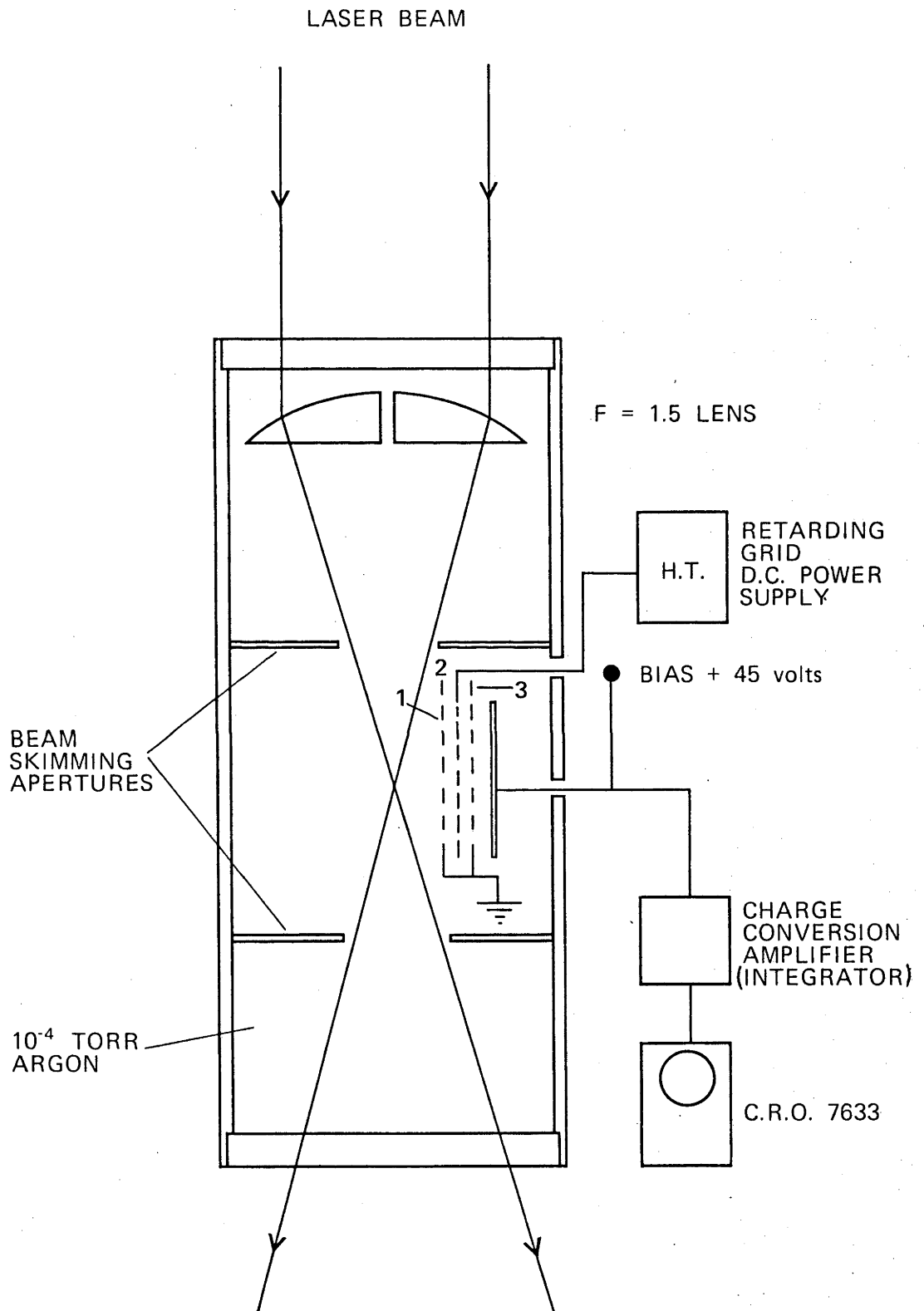


fig. 3,7: TEST CHAMBER DETECTOR ARRANGEMENT

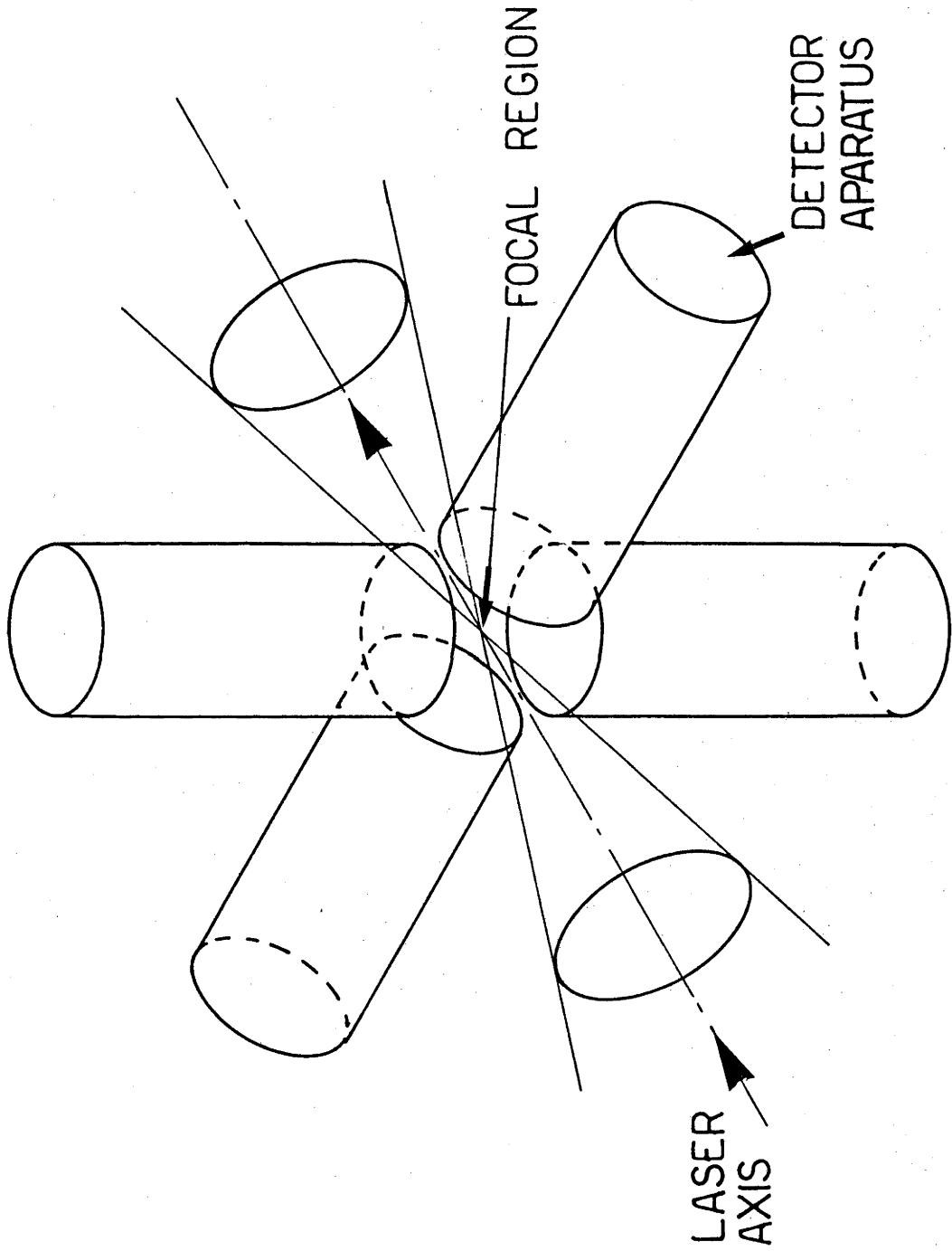


fig.3,8: MULTIDIRECTIONAL ANALYSER CONFIGURATION

This allowed the electron yield to be monitored separately at different orientations to the laser polarization (vertical in this experiment) although this facility was not used. All four detectors were connected in parallel to increase the total signal available. Each detector consisted of three grids and a collector plate as shown in fig. 3.7. The first and third grids were grounded and the second was biased to act as a retarding grid using a high voltage D.C. power supply. Hollis (1978) tested the analyser using an electron gun which produced a $50 \mu\text{A}$ beam of $20 \pm 5 \text{ eV}$ electrons, and no electrons (less than 0.2 nA) reached the collector when the retarding grid potential exceeded the maximum electron energy. The collector itself was biased at $+45$ volts to prevent secondary electron losses.

The current incident on the collector was amplified by the charge conversion amplifier, integrated, and the output signal displayed on a Tektronix 7633 oscilloscope. The integrator decay time was several microseconds and a typical display is shown in fig. 3.4b. The C.R.O. was triggered 50 ns before the electron signal arrived and the height of the pulse to the plateau region was measured in millivolts. The detector system sensitivity was 1.2×10^{-15} coulombs per millivolt (7.5×10^3 electrons per millivolt). Some low frequency mains pick-up ($\sim 100 \text{ Hz}$) resulted in shot-to-shot shifting of the baseline by $\pm 5 \text{ mV}$. High frequency noise on the time scale of 50 ns per division was measured at 1 mV (7.5×10^3 electrons) and this determined the detection limit for the experiment. The output of the detection system was designed to be linear within the one volt signal range expected.

Detection of the minimum charge at the collector required that more than the minimum detectable number of electrons be produced in the focal region, since not all such electrons reached the detector. This was due to the detector geometry which did not completely surround the focal region. Each collector plate had a diameter of 3.0 cm and was located 3.2 cm from the focal region, giving a combined solid angle of 2.8 steradians for the four detectors. Assuming that the electrons were accelerated isotropically from the focal region, and since each grid had a (measured) transmission fraction of 0.9 , then the fraction Ω of electrons reaching the collector was

$$\begin{aligned}\Omega &= 2.8 \times (0.9)^3 / 4\pi \\ &= 0.16 \dots\dots\dots 3.3\end{aligned}$$

Thus in order to register the minimum charge N on the collector, $N/\Omega = 4.6 \times 10^4$ electrons must be produced in the focal region. At a pressure of 10^{-4} torr this corresponds to a fully (singly) ionized volume of $1.4 \times 10^{-8} \text{ cm}^3$ of gas. This is referred to as the minimum volume necessary to produce a detectable charge on the collector. From fig. 3.6 it can be seen that on the surface enclosing the minimum volume, the intensity will be only 0.43 that of the central intensity (measured by the laser diagnostics). Hence the intensity at which electrons are first detected must be multiplied by this correction factor to give the

ionization threshold intensity. As a consequence of the minimum volume, electrons generated in the very highest intensity regions of the beam will not be detected.

6. PRESSURE CONSIDERATIONS

The pressure to which the test chamber was filled with argon was determined as a compromise between competing considerations. The number density had to be sufficiently high in order firstly that sufficient signal be obtained from the detector, and secondly so that electrons ionized from impurity gases within the chamber contributed negligibly to the total signal output. While the filling lines and chamber were flushed with argon and pumped down several times to the chamber base pressure (10^{-6} torr), and the chamber 'baked' for long periods of time, impurity gases were still present in the chamber. Since nitrogen and oxygen ionization potentials are lower than for argon (see IV.2), the argon pressure must be several orders of magnitude larger (at least 10^{-4} torr) in order that the electron contribution from the impurities be small compared with that of argon. This was tested by firing the laser prior to filling with argon and measuring the resultant signal.

Competing with the need for adequate electron signal were the effects of the interaction of electrons with other particles. The overriding requirement was that electrons accelerated from the focal region reached the detector without any change in velocity and without causing collision induced ionization. The various mechanisms involved are treated below.

(i) Mean Free Path: In calculating the mean free path (λ_f) the effect of small deflections ($< 90^\circ$) must be considered in addition to large collisions (90°) due to the long range of electrostatic forces (Spitzer, 1962). When only the latter are included the electron mean free path (electron-electron and electron-neutral collisions are negligible) is

$$\lambda_f(90^\circ) = (n\pi\rho^2)^{-1} \dots\dots\dots 3.4$$

where n = argon number density ($3.3 \times 10^{12} \text{ cm}^{-3}$)

ρ = impact parameter

$$= \frac{Ze^2}{4\pi \epsilon_0 mV^2}$$

V = electron velocity

which gives $\lambda_f = 32$ cm for 1 eV electrons. For small deflections however

$$\lambda_f(<90^\circ) = \frac{\lambda_f(90^\circ)}{8 \ln \Lambda} \text{ cm} \dots \dots \dots 3.5$$

where $\ln \Lambda$ is the Coulomb logarithm (of order 10 in this case). This gives a λ_f of ~ 4 mm which is much less than the chamber dimensions. However, it is much greater than the dimensions of the focal volume (several hundred microns) and after travelling this distance, the ponderomotive force will have accelerated the electron to much higher energies. Since no ions existed outside the focal region then it may be assumed that at 10^{-4} torr no collisions occurred to alter the electron energy spectra.

(ii) **Avalanche Breakdown Threshold:** In the focal region, electrons accelerated by the electric field that might collide with argon atoms could produce additional electrons in a cascade ionization process. The threshold intensity at which this occurs in the low pressure, short pulse case where neither diffusion nor recombination is important is given by (Hughes, 1975)

$$I_A = \frac{n}{c} \left(\frac{\omega}{v_f} \right)^2 \frac{1}{\tau} \ln(i_B V_f n) \text{ W cm}^{-2} \dots \dots \dots 3.6$$

where

- n = number density ($3.3 \times 10^{22} \text{ cm}^{-3}$)
- c = $2.6 - 3.8 \times 10^{21}$ for Ar
- ω = $1.77 \times 10^{15} \text{ rad s}^{-1}$ for Nd:Yag
- v_f = collisional frequency
- = electron velocity / λ_f
- τ = laser pulse duration (25 ps)
- i_B = degree of ionization (10^{-3})
- V_f = e^{-1} focal volume ($\sim 2 \times 10^{-8} \text{ cm}^3$)

For 1 eV electrons (which give the lowest threshold) $I_A \sim 3 \times 10^{16} \text{ W cm}^{-2}$.

Since the majority of electrons had energies greater than 1 eV and since the laser intensity necessary to produce 1 eV electrons was less than I_A , no avalanche breakdown effects occurred at 10^{-4} torr.

(iii) Electron-ion Coupling: Electrostatic coupling between electrons and ions resulting in transfer of the electron energy to ion motion is another mechanism which may affect the electron energy spectra. The effect of this has been studied by Boreham and Luther-Davies (1979) and Boreham and Hora (1979) and is the major limitation on the upper chamber pressure level. Boreham and Hora's plot of the number of electrons with energy greater than 50 eV as a function of pressure for a constant intensity in helium revealed a departure from a linear relationship at pressures above $1.6 \pm 0.5 \times 10^{-4}$ torr. This indicated that fewer electrons per neutral were reaching the detector as would be expected if electrons lost sufficient energy to ions to be repelled by the retarding grid.

Theoretical considerations of the Debye length λ_D (the parameter governing electron-ion coupling) can also give a general estimate of the upper pressure limit. By definition (Delacroix, 1965)

$$\lambda_D = \left(\frac{kT}{4\pi e^2 zn} \right)^{1/2} \text{ cm} \dots\dots\dots 3.7$$

where T = electron temperature ($^{\circ}$ K)
 k = Boltzmann's constant
 n = ion number density ($3.3 \times 10^{12} \text{ cm}^{-3}$)
 z = ionic charge

This can be re-written as

$$\lambda_D = 743.4 \left(\frac{2}{3} \frac{\xi_{\text{KIN}}}{nz} \right)^{1/2} \text{ cm} \dots\dots\dots 3.8$$

where ξ_{KIN} is the electron kinetic energy in electron volts and λ_D is in cm. For 1 eV electrons this gives ($z = 1$) a Debye length of $\sim 3 \mu\text{m}$ compared with the focal diameter of $\sim 13 \mu\text{m}$. Thus some electron ion coupling would be expected before the electrons are accelerated from the focal region by the ponderomotive force.

However, a kinetic energy of 1 eV is a pessimistic estimate of the electron energy since the electron is being continuously accelerated in the beam. This is particularly true for high intensity pulses where an electron does not have to move far in order to experience a substantial drop in the electric field intensity. An upper limit is to assume that the electron attains its energy due to the ponderomotive force the instant it is ionized. The energy attained is then equal to the oscillation energy of the electron at that point in the beam, i.e. from 2.42

$$\begin{aligned} \xi_{\text{KIN}} &= \xi_{\text{OSC}} \\ &\sim 10^{-13} \text{ eV} \dots\dots\dots 3.9 \end{aligned}$$

where I is measured in W cm^{-2} .

$$\text{Thus } \lambda_D' = 743.4 \left(\frac{2}{3} \frac{\xi_{\text{OSC}}}{n z} \right)^{1/2} \text{ cm} \dots\dots\dots 3.10$$

$$\sim 2 \times 10^{-4} \left(\frac{I}{n z} \right)^{1/2} \text{ cm} \dots\dots\dots 3.11$$

The Debye length may now be equated to the diameter of the focal volume in order to define a characteristic number density (and hence pressure) above which electron-ion coupling would be certain to occur. This is given by

$$n^* \sim 3.7 \times 10^{-8} \frac{I}{z d^2} \text{ cm}^{-3} \dots\dots\dots 3.12$$

$$\text{that is } p^* \sim 1.12 \times 10^{-24} \frac{I}{z d^2} \text{ torr}$$

$$\sim 6.6 \times 10^{-19} \frac{I}{z} \text{ torr} \dots\dots\dots 3.13$$

using $d \sim 13 \mu\text{m}$.

For an intensity of $3 \times 10^{15} \text{ W cm}^{-2}$ as used in Boreham and Hora (1979) this gives (for single ionization) a pressure of $p^* \sim 2.0 \times 10^{-3} \text{ torr}$ as the upper limit.

Thus the result of Boreham and Hora (1979) of $1.6 \pm 0.5 \times 10^{-4} \text{ torr}$ can be seen to lie below this. In fact the upper limit is obviously overestimated since using $I = 3 \times 10^{15} \text{ W cm}^{-2}$ assumes an electron energy of $\sim 300 \text{ eV}$ whereas in fact only electrons of energy greater than 50 eV were considered. These 50 eV electrons define a pressure of $3.3 \times 10^{-4} \text{ torr}$ above which electron-ion coupling would be expected and this is closer still to the quoted result.

In this experiment intensities of greater than $3 \times 10^{14} \text{ W cm}^{-2}$ were used corresponding to an upper limit of $2 \times 10^{-4} \text{ torr}$. Since chamber pressure was a factor of two below this then Debye coupling could be expected to have had a negligible effect on high energy electrons. For electron energies of less than 20 eV , however, for which p^* is of the order of 10^{-4} torr or less, some electron-ion coupling may have occurred. The electron loss was not significantly great in the region near the threshold pressure shown in Boreham and Hora (1979) and it is this compromise that was made in order to obtain adequate electron signal.

CHAPTER IV

RESULTS

1. INTRODUCTION

Almost a thousand shots were taken using the SPL laser with measurements of electron yield, laser energy, pulse duration and retarding potential tabulated for each one. The laser energy monitor was corrected for spurious pick-up from the A45 amplifier whenever this occurred by comparison with the pulse height detector. Laser peak central intensities of between 3×10^{14} and $4 \times 10^{16} \text{ W cm}^{-2}$ were observed, giving detector signals of up to 3.6×10^6 electrons (480 mV) which was within the region of linearity of the charge conversion amplifier. The mean pulse length was 22 ps with over 90% of pulses being between 18 and 36 ps in a distribution somewhat similar to Luther-Davies (1977).

2. BACKGROUND TESTING

Prior to filling the test chamber with argon to 10^{-4} torr the laser was fired into the 10^{-6} torr impurity gas to determine the contribution of background signal. This was carried out over the full range of laser intensities and the integrated electron energy spectra obtained for each intensity. No background signal was obtained for intensities less than $2 \times 10^{15} \text{ W cm}^{-2}$.

On the same timescale as used for the detector signal in argon (50 ns/division), the unretarded background signal was measured at $\sim 10\%$ of the argon signal for intensities in the range $5 - 20 \times 10^{15} \text{ W cm}^{-2}$, and at around 20% at the highest intensity setting ($3 - 4 \times 10^{16} \text{ W cm}^{-2}$). However, the signal was a lesser percentage of the equivalent argon signal when the electrons were retarded, and disappeared altogether at less than one tenth the maximum retarding voltage in argon. Since the background electrons were all collected over a short time (< 50 ns) then time-of-flight calculations indicate that at energies of a few eV, these electrons were ionized within the focal region. The electrons would probably have originated from nitrogen and oxygen atoms rather than molecules due to the relatively low dissociation energy of these gases (9.8 and 5.2 eV respectively - Weast, 1974) in comparison with their molecular ionization potentials (15.6 and 12.1 eV). Thus dissociation of the molecules would have occurred early in the pulse, followed by ionization of the nitrogen and oxygen atoms (with ionization potentials of 14.5 and 13.6 eV respectively).

However, the results obtained at the highest intensity setting showed a larger second signal that occurred $1 - 2 \mu\text{s}$ later (when viewed on a scale of $2 \mu\text{s} / \text{division}$). The later signal disappeared for a lower retarding voltage of -30 to -50 V in comparison with the first signal ($\sim -100 \text{ V}$).

In order to investigate this, detector signals were also recorded on longer time scales ($2 \mu\text{s} / \text{division}$) during the experiment with argon, and the results clearly indicated two separate signals. The first occurred with a sharp rise time (corresponding to electrons ionized within the focal region), while the second was much larger and occurred $\sim 4 \mu\text{s}$ after the first. This was observed for intensities above $10^{15} \text{ W cm}^{-2}$ and became much greater in proportion to the first signal as the laser intensity increased. For the highest intensity shots, the plateau region of the first signal on a short time scale was no longer flat due to the size of the following signal, which appeared to start soon after and peak $\sim 5 \mu\text{s}$ later. In all cases the second signal was completely eliminated when a retarding potential of -10 V was applied, and the remaining signal corresponded to the equivalent retarded signal on the $50 \text{ ns} / \text{division}$ trace. A detailed analysis of the integrated electron spectra at the highest intensity showed that only $1 - 2$ volts were required to eliminate most of the second signal.

It is doubtful whether the later signal originated from surface ionization effects within the chamber, since the signal was much larger (by a factor of ~ 5) when argon was present at the same intensity. The detectors were also shielded by the beam skimming apertures and in any case, the laser intensity (unfocussed) on the chamber surfaces would be too low to cause significant ionization. Hence the second signal, like the first, must have been due to ionization of the gas in the chamber. The fact that the signal was not ~ 100 times greater at the higher pressure (in keeping with the pressure ratios) could be due to the lower ionization potential of the impurity gases which would greatly increase their ionized volume in comparison to that for argon at the same intensity.

The presence of the later signal could be explained in terms of electron-ion coupling which would significantly reduce the electron velocity. To check this, an ion trace was taken in argon using the highest amplifier setting. The ion signal peaked $\sim 3 \mu\text{s}$ after the start of the first electron signal thus coinciding approximately with the arrival of the second electron signal. This indicated that electron-ion coupling had indeed occurred, and an explanation of the behaviour of the later signals can be found in the Debye length analysis of III.6.

At high laser intensities, low energy electrons originate from far out in the focal volume. This increases the strength of Debye coupling since the focal diameter is larger and higher electron energies are needed to satisfy the relation 3.8. Hence, at high intensities, significant Debye coupling would occur over a large energy range at the low end of the energy spectra, and this would be expected to increase the late signal in relation to the uncoupled early signal as the intensity is increased. This agreed with the observations above.

Further, since $\lambda_D^2 \propto \xi_{\text{KIN}} / n$, a lowering of the number density n by two orders of magnitude would increase the Debye length λ_D by a factor of 10 for a given electron energy. Thus Debye coupling would be weaker and would be expected only at the highest intensities where the focal volume is large enough to approach the Debye length. This too was verified by the appearance of the second signal at higher intensities in the background gas ($> 10^{16} \text{ W cm}^{-2}$) than in argon ($> 10^{15} \text{ W cm}^{-2}$).

There was an inconsistency, however, in the voltage required to suppress the coupled electrons (30 to 50 V in some cases) compared to the energy associated with electrons travelling at the ion velocity from the focus ($\sim 0.01 \text{ eV}$). This could not be explained by the presence of electrons originating from elsewhere in the chamber since for energies of $\sim 30 - 50 \text{ eV}$, time-of-flight calculations would imply that they originated from several metres outside the chamber. This discrepancy was resolved by examination of the mesh spacing in the grid of the retarding field analyser. When a quasi-neutral gas cloud is incident on the analyser it will efficiently separate the electrons from the ions provided the Debye length in the cloud is much larger than the mesh spacing. This condition was not satisfied by the detector used and hence a sufficiently low retarding potential could be penetrated by the electron-ion cloud because of the formation of charge separation fields. On reaching the collector the ions would be repelled by the +45 V bias and the electrons corresponding to the late (coupled) signal would be detected.

It is clear from analysis of the background testing that the presence of impurity gases in the chamber was the cause of the background electrons detected. It is also apparent that the background electrons contributed to the integrated (argon) electron energy spectra where it matters least (see fig. 2.2). Since the maximum background electron energy was always much less than one tenth that in argon the high energy end of the electron spectra was unaffected, and it was this region that was used to determine the onset of ionization. At low intensities, where even low energy contributions to the spectra are important, no background signal was observed at all. Thus the presence of a background electron signal originating from impurity gases would not affect the determination of ionization intensity thresholds due to the nature of the electron energy technique employed.

3. EXPERIMENTAL RESULTS

Each data point acquired was the average of 4 shots taken at each amplifier and retarding voltage setting. This was done to reduce random scatter due to the large errors involved. Three sample electron energy contours at 0, -20 and -140 volts are shown in fig. 4.1. The electron yield N_e is plotted against the laser intensity for each shot and the mean of the four data points is shown together with the standard deviation of the points

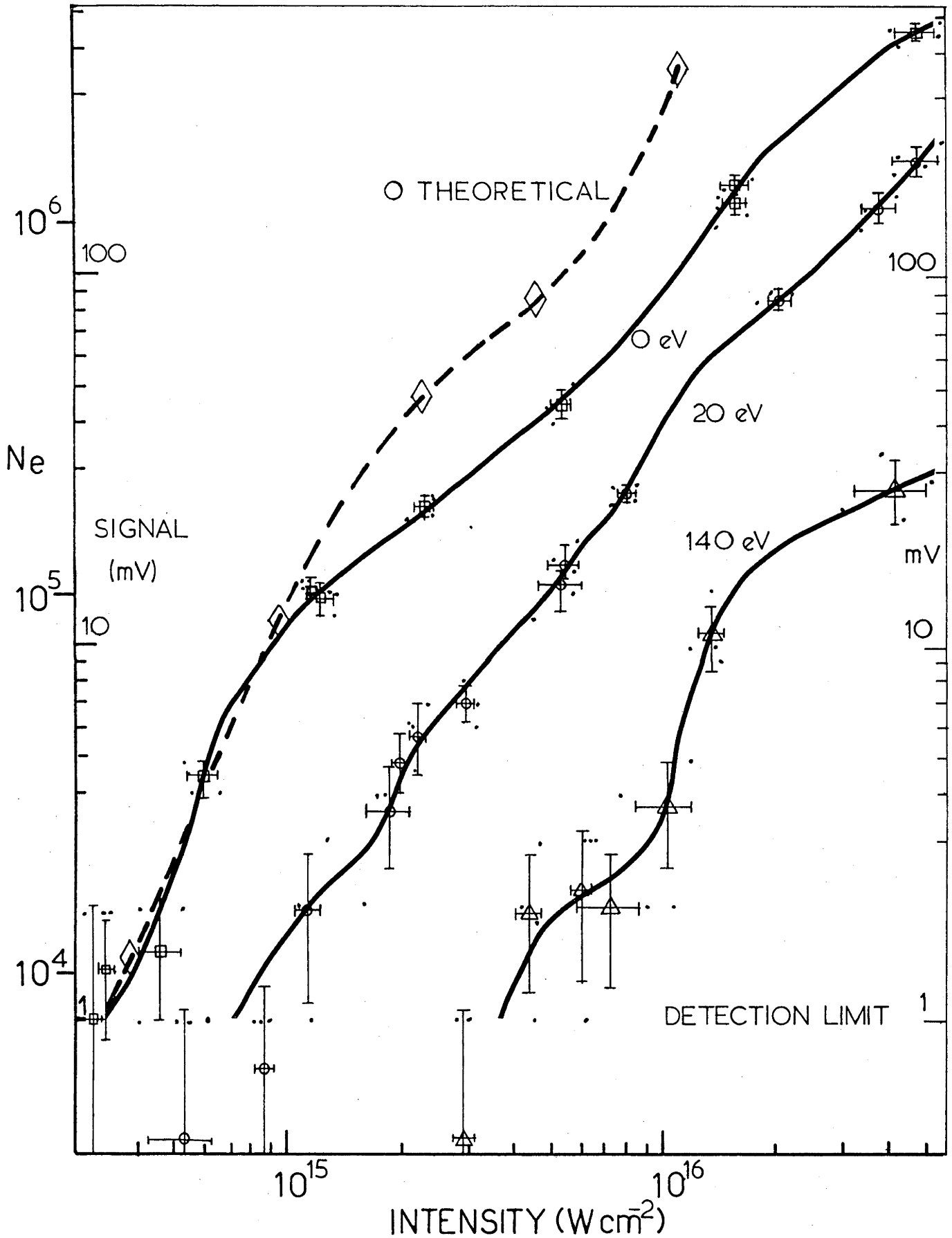


fig. 4,1: SAMPLE ELECTRON ENERGY CONTOURS

from the mean. Also shown is the expected zero retarding potential yield assuming (1) an apparent threshold intensity of $3 \times 10^{14} \text{ W cm}^{-2}$, (2) a correction factor for this of 0.43, and (3) the volume versus relative intensity diagram of fig. 3.6.

The standard deviation does not necessarily reflect the error in the measurement since the scatter in the data points can be due to shot-to-shot variation in the laser intensity. An indication of the error in the electron yield is given by the second scale on the vertical axis in fig. 4.1, which shows the detector signal in millivolts. The noise level of one millivolt defined both the detection limit and the error in N_e . Since some shots resulted in no detectable signal the mean of some sets of data points fell below the detection limit.

The random error in the intensity was the same for all measurements and was a combination of independent errors in pulse length and laser energy. The TPF monitor traces were measured to an accuracy of 10% and the laser energy (as measured by the pulse energy integrator after correction for spurious pick-up) was accurate to within 5%. This gave a random error in the laser intensity of around 12%. An overall systematic error in the laser central intensity may have resulted from inaccuracy in the measurement of the e^{-1} focal diameter ($13 \pm 2 \mu\text{m}$ — see equation 3.2) which could shift the horizontal scale by as much as -25% to $+40\%$. Pressure fluctuations not resolved by the 20% accuracy of the Varian gauges may have caused a random uncertainty in the electron yield, and may also have caused a systematic error in the correction factor 0.43 if the calibration was in error by $\pm 20\%$.

Despite the attempt at reducing the random error by plotting the mean of the four data points in each group, fig. 4.1 shows that there was still considerable scatter in the means, particularly near the detection limit. Nevertheless, all electron energy contours plotted through the mean line of best fit were self-consistent since they did not overlap. The electron energy contours for all values of the retarding potential are shown in fig. 4.2. The lines of best fit through the means for a given retarding potential were supplemented by interpolation between adjacent contours.

From the contours of fig. 4.2 can be derived the integrated electron energy spectra of fig. 4.3. These were obtained by plotting (for a fixed intensity) the electron yield as a function of retarding potential. The random error and detection limit remained the same as for the electron energy contours while the electron energy (retarding potential) was accurate to within 1%.

As outlined in II.6, the electron energy contours and integrated electron spectra can be used as semi-independent means of determining the ionization threshold intensities. Considering firstly fig. 4.2, a bunching of the electron energy contours can be seen to occur most noticeably at around $3 \pm 0.5 \times 10^{14} \text{ W cm}^{-2}$ and $9 \pm 2 \times 10^{14} \text{ W cm}^{-2}$, with the

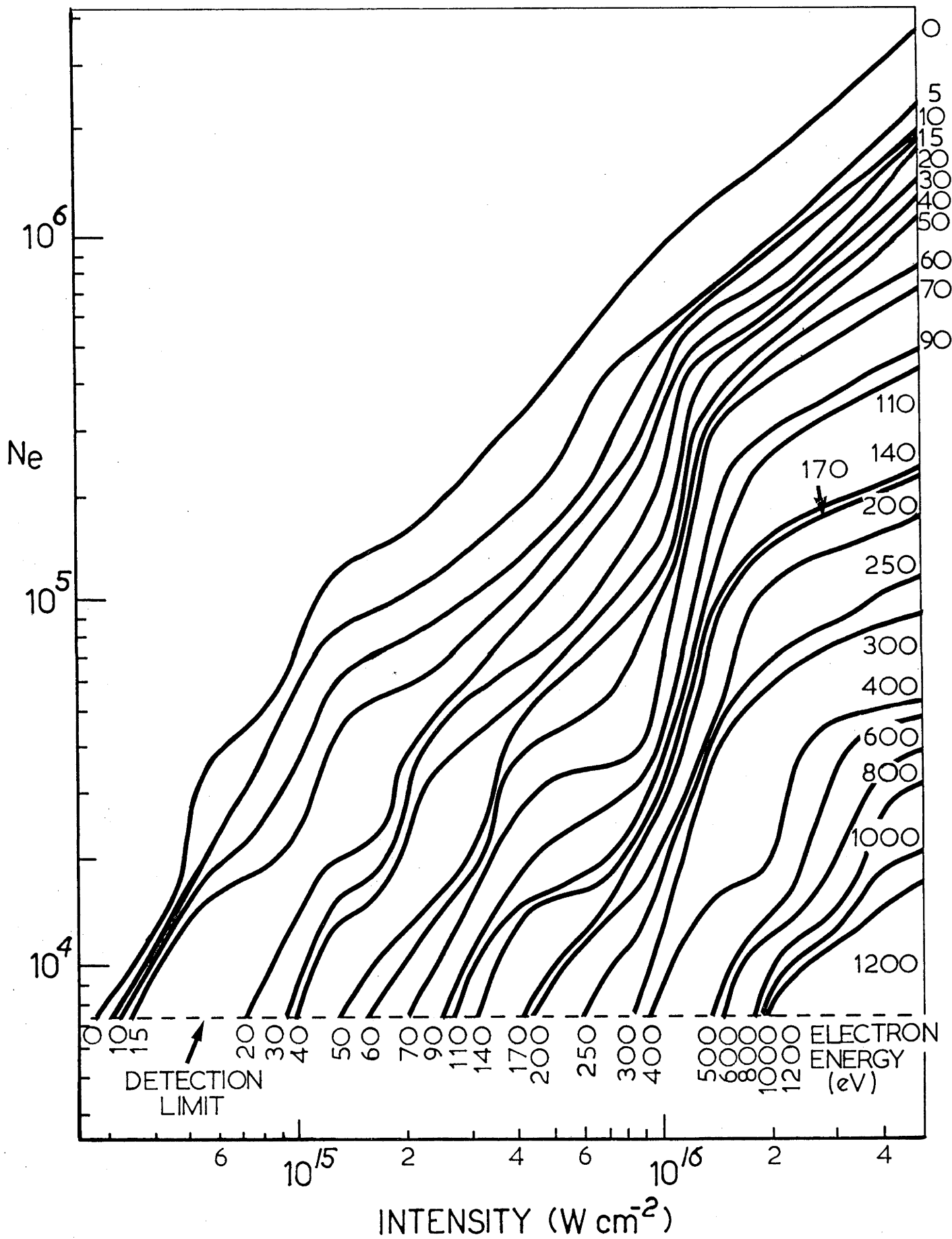


fig. 4.2 ELECTRON ENERGY CONTOURS

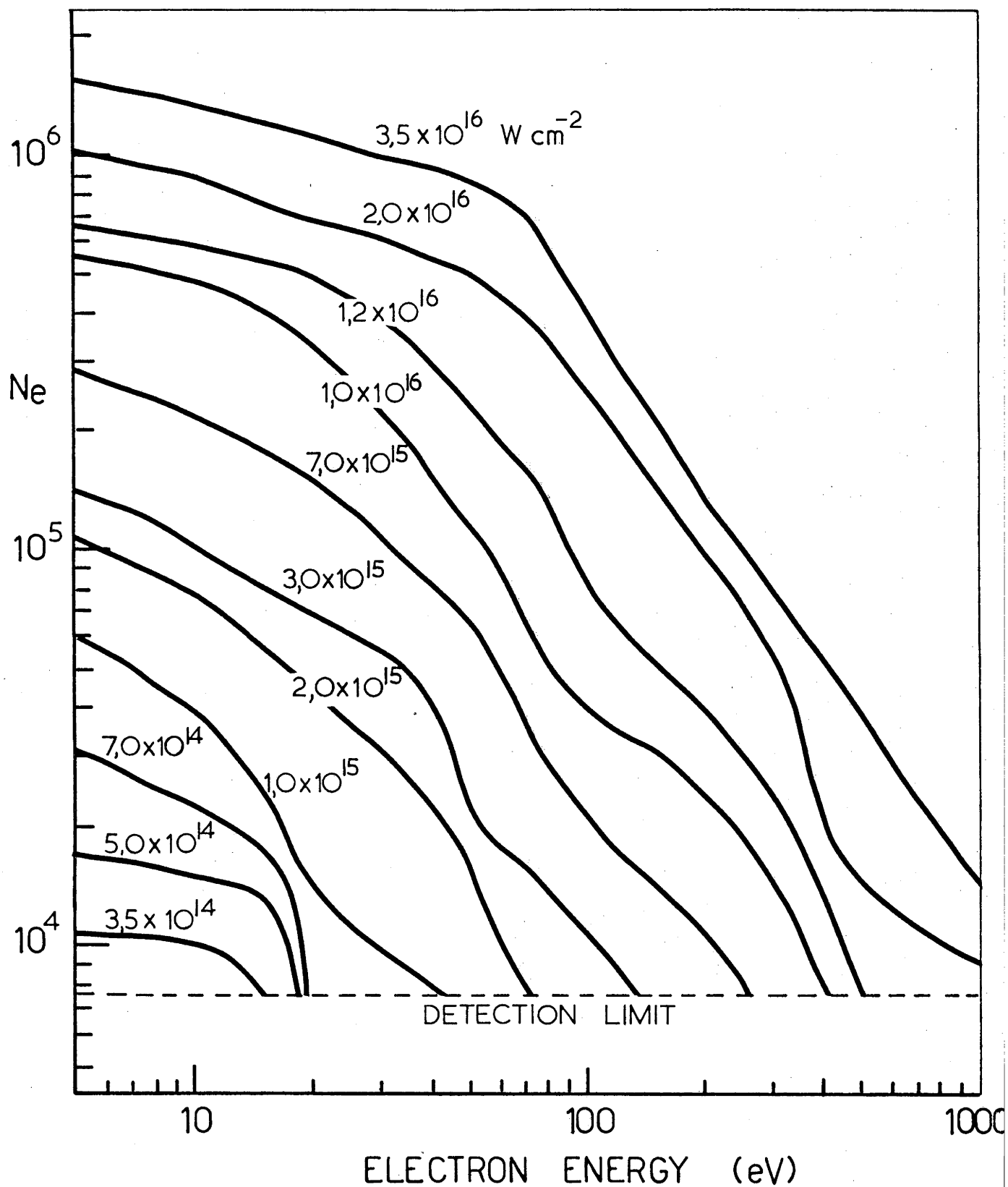


fig. 4,3 INTEGRATED ELECTRON ENERGY SPECTRA

possibility of a third at $1.8 \pm 0.6 \times 10^{16} \text{ W cm}^{-2}$. In view of the large errors near the detection limit it must be stressed that these observations should be treated with caution, although some confidence could be placed in the first two which were relatively well defined. When the correction factor 0.43 is applied the results yield ionization intensity thresholds of $1.1 - 1.5 \times 10^{14} \text{ W cm}^{-2}$, $3 - 5 \times 10^{14} \text{ W cm}^{-2}$ and $0.5 - 1.0 \times 10^{16} \text{ W cm}^{-2}$.

Examination of fig. 4.3 reveals the possibility of ionization thresholds in the integrated electron spectra at 12 – 20 eV ($1.2 - 2.0 \times 10^{14} \text{ W cm}^{-2}$) and (less clearly) at 30 – 80 eV ($3 - 8 \times 10^{14} \text{ W cm}^{-2}$) and 250 – 600 eV ($2.5 - 6 \times 10^{15} \text{ W cm}^{-2}$). The first two of these agree well with the first two thresholds given by the electron energy contours and can be assumed to indicate the same ionization states. The last threshold from each method may, however, indicate different ionization states as the intensity ranges do not overlap to the same extent.

Since the integrated spectra did not give a clear indication of the ionization thresholds, the curves of fig. 4.3 were differentiated to give the actual electron energy spectra of fig. 4.4. The ionization states would be expected to appear as peaks in the spectra corresponding to groups of electrons with velocities related to the ionization thresholds by equation 2.42. As can be seen from figs. 4.4a and 4.4b, the peaks for the 30 – 80 eV and 250 – 600 eV states respectively are readily apparent as the laser intensity increases and give a clearer physical indication of the onset of ionization in higher states. The 12 – 20 eV state is indicated by the off-scale peak in fig. 4.4a, while the presence of yet another state is indicated by a slight inflection in the $10^{16} \text{ W cm}^{-2}$ curve, and perhaps by the presence of the plateau in the 100 – 250 eV region. However, it must be mentioned that the errors involved in estimating slopes cause the spectral peaks to be qualitative indicators only of the presence of ionization states.

It is not clear from the analysis above which of the ionization thresholds from either technique correspond to the various ionization states of argon. The situation is clarified, however, by the results of Boreham (1979c) who observed (spectra) thresholds for HeI and HeII at 25 – 80 eV ($2.5 - 8 \times 10^{14} \text{ W cm}^{-2}$) and 200 – 1000 eV ($0.2 - 1.0 \times 10^{16} \text{ W cm}^{-2}$). He also observed two clear bunchings of the electron energy contours at $8 \pm 2 \times 10^{14} \text{ W cm}^{-2}$ and $8 \pm 2 \times 10^{15} \text{ W cm}^{-2}$ corresponding to ionization thresholds of $2.6 - 4.3 \times 10^{14} \text{ W cm}^{-2}$ and $2.6 - 4.3 \times 10^{15} \text{ W cm}^{-2}$. The agreement of the two techniques for helium and the large separation of the ionization thresholds clearly indicates the presence of the HeI and HeII states. These are plotted (solid symbols) in fig. 4.5 which also shows the ionization threshold intensity required for a given ionization potential based on the theoretical calculations of II.5.

The results in helium now assist in the interpretation of the argon data shown in fig. 4.5 (hollow symbols) due to the proximity of ArII to HeI and of ArIV to HeII. The first result of each technique corresponds to ArI (whose threshold is less than for HeI),

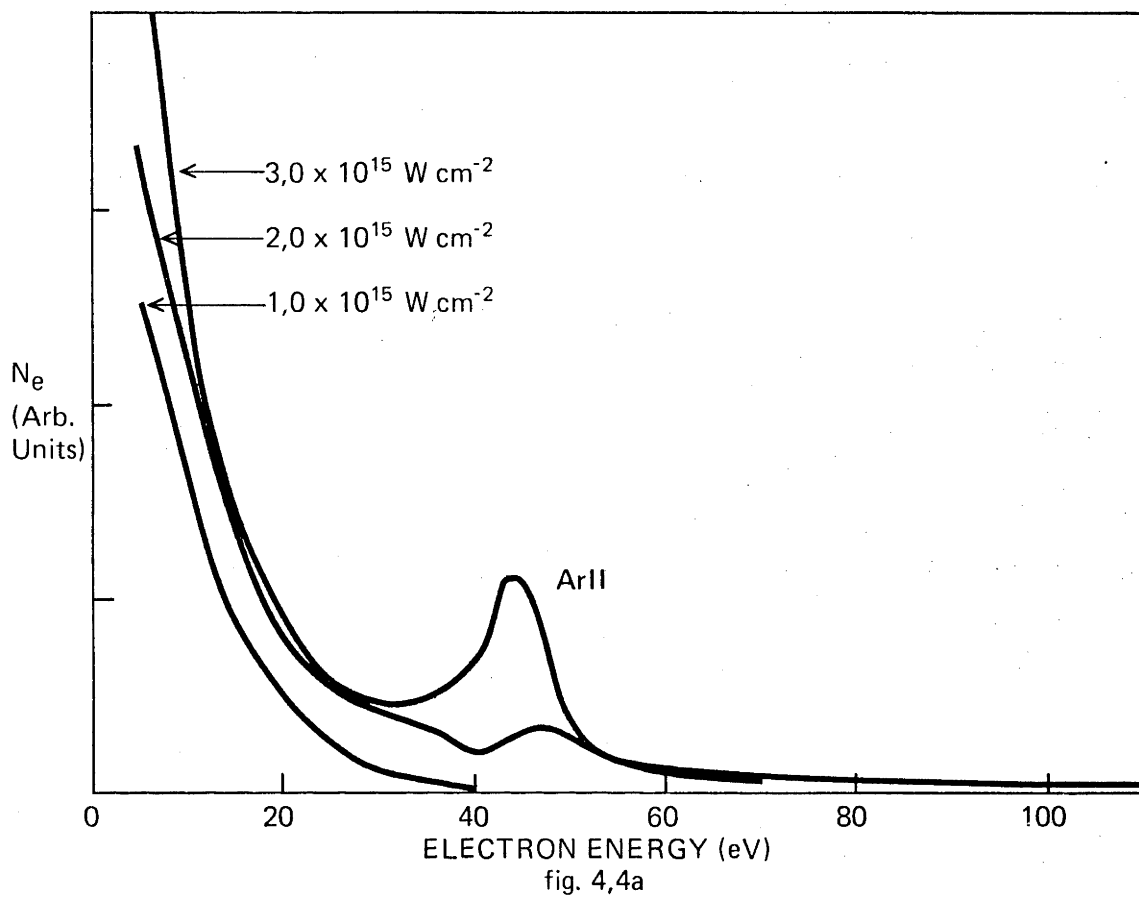
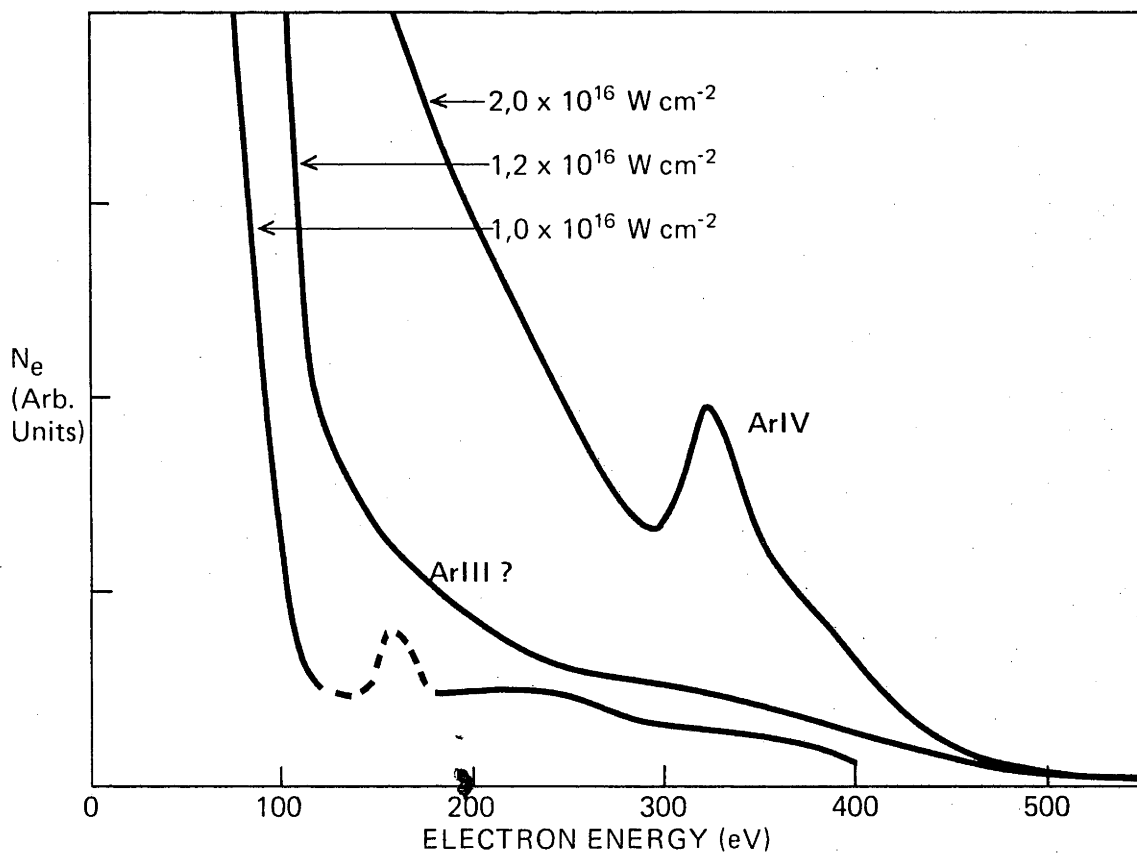


fig. 4,4a

fig. 4,4b: SAMPLE ELECTRON ENERGY SPECTRA

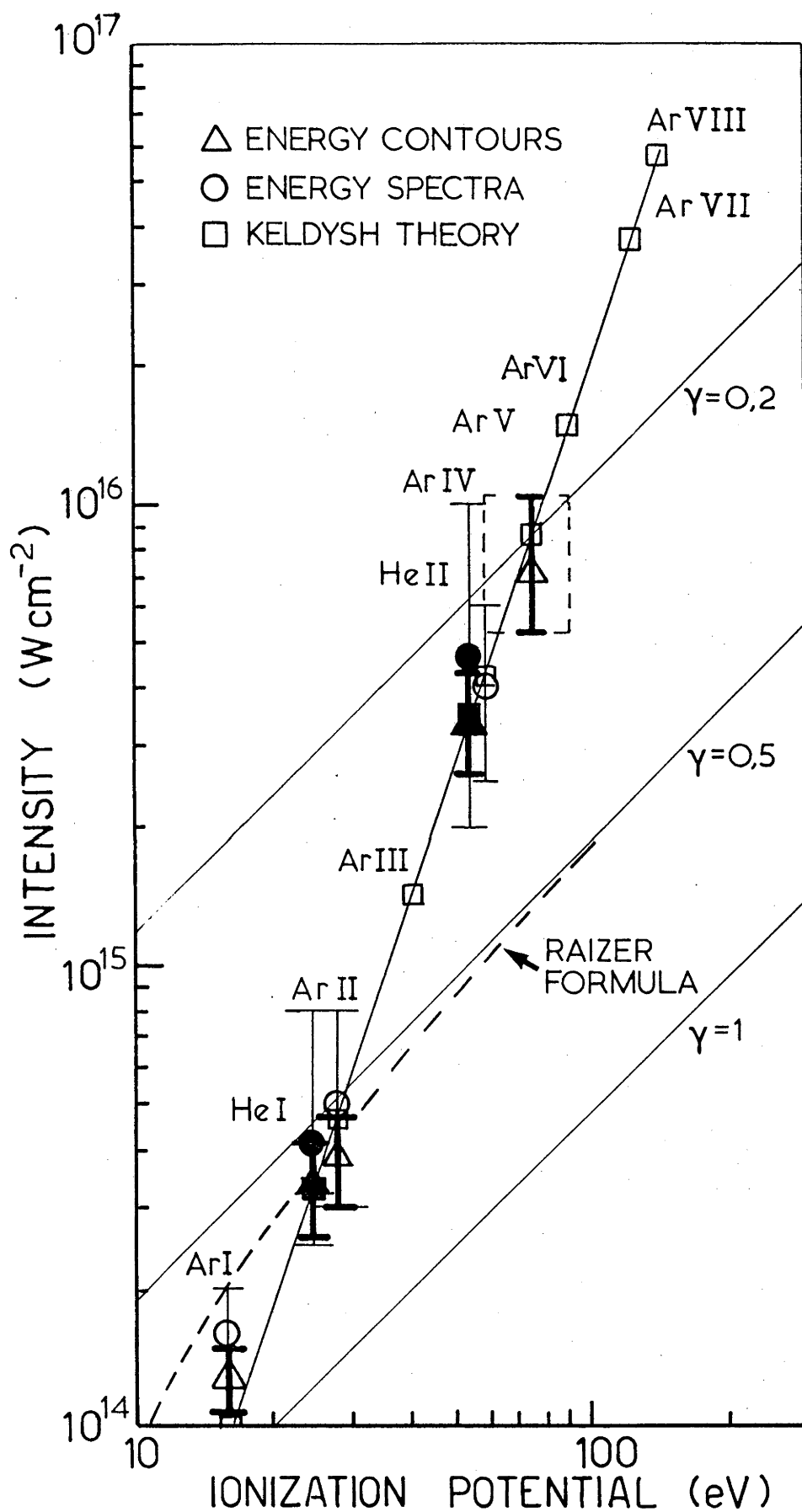


fig. 4.5: EXPERIMENTAL AND THEORETICAL IONIZATION THRESHOLD INTENSITIES

while the second of each set of results corresponds to ArII. The small peak and plateau in fig. 4.4b perhaps indicate the presence of the ArIII threshold at the expected level ($1 - 2.5 \times 10^{15} \text{ W cm}^{-2}$ c.f. $1.5 \times 10^{15} \text{ W cm}^{-2}$ from calculation) but the errors in this region are too large to confidently place this state in fig. 4.5. The last result from the electron spectra ($2.5 - 6 \times 10^{15} \text{ W cm}^{-2}$) can be seen to correspond best to ArIV, particularly in view of the proximity of the HeII result. However, the last energy contour result ($0.5 - 1.0 \times 10^{16} \text{ W cm}^{-2}$) could correspond to any of the ArIV - VI states as indicated by the dashed box, although the vertical error bar is placed on the most likely state (ArV). The ArV result is further supported by the behaviour of the integrated spectra at $\sim 1 \text{ keV}$ which are similar in shape to those near the ArII threshold, thus indicating the presence of the next ionization state (ArV).

The smaller vertical error bars for the energy contour results in fig. 4.5 indicate a greater apparent accuracy for this method, although the appearance of ionization states is more evident from the actual electron spectra. However, the electron contours may be subject to a greater systematic error in the estimation of the minimum volume correction factor (0.43). The uncertainty in this is difficult to evaluate due to an incomplete knowledge of the isotropic (or otherwise) acceleration of electrons from the focal region.

4. DISCUSSION

Comparison of the idealized and actual integrated electron energy spectra of fig. 2.2 and fig. 4.3 indicates a significant departure from the expected behaviour in the experimental results. Apart from the bunching of the spectra for the first ionized state, the existence of higher states is far from apparent when the size of the errors in the region near the detection limit is considered. However, plotting of the actual electron spectra enhances the resolution of the ionization thresholds slightly. A similar difficulty is encountered in the analysis of the electron energy contours of fig. 4.2 where only the first, second and fourth ionization states can confidently be determined. Thus considerable caution must be exercised when interpreting the results summarized in fig. 4.5 despite the attempt to convey this uncertainty through the use of the large error bars shown.

The cause of the departure from the idealized electron energy contours can be found in a closer examination of the approximations made in II.6 and III.6. Consider firstly the discrepancy between the observed unretarded electron energy contour and the expected result shown in fig. 4.1. The theoretical curve was based upon the assumption of a minimum volume correction factor of 0.43 and on the validity of the iso-intensity contour diagram of fig. 3.5. The latter may be open to question due to the difficulty in measuring the outermost contours in the original experiment (Boreham and Luther-Davies, 1979) since they were less well defined than those near the central intensity point. The points

marked on the predicted unretarded curve correspond to the iso-intensity contours of fig. 3.5, and a departure from the curve occurs outside the second innermost (0.15) contour. It is from here that the iso-intensity contours also start to expand rapidly. Hence an error in their measurement would result in a large overall error in the volume which they enclosed, although possibly not by the factor of 2 – 3 needed to account for the discrepancy.

Alternatively, the estimate of the minimum volume correction factor may be incorrect, and in fact if the expected curve were shifted downward a closer fit to the data occurs. However, this would imply a smaller correction factor than 0.43, whereas fig. 4.5 indicates that in the cases where both integrated spectra and energy contours are available, the centroid of the error bar for the energy contours is lower than that for the spectra. Since the spectra provide a more direct measure of the ionization threshold than the minimum volume correction factor is, if anything, too low. It is conceivable too that the correction factor (0.43) may change with intensity as the low energy electron component (making up the bulk of the signal) originates from further out in the focal volume. From fig. 3.5 it can be seen that the intensity gradient is axial for most of the electrons produced in the region outside the 0.15 contour. Hence as the intensity increases, more electrons are accelerated axially and a lower percentage reach the detector.

Another explanation may be found in the electron-ion coupling effects discussed in IV.2. It was noted that a late electron signal was observed (corresponding to the ion pulse) for intensities above $10^{15} \text{ W cm}^{-2}$ and hence for intensities below this no detectable electron-ion coupling occurred. Thus no signal loss would be expected for intensities below $10^{15} \text{ W cm}^{-2}$, while a gradual loss in the early signal due to the retarding effect of the ions would be expected above this intensity. This is in exact agreement with the departure of the expected curve from the experimental results shown in fig. 4.1. While Debye coupling would be expected for low energy electrons over all intensity ranges, the relation 3.8 indicates (IV.2) that the coupling strength increases at higher intensities due to the increase in the focal dimensions. The dimensions do increase significantly beyond the 0.15 contour and the stronger coupling this implies would retard a greater range of electron energies. In addition, the proportion of low energy to high energy electrons increases thereby increasing the proportion of electrons susceptible to retardation.

Electron-ion coupling may also explain the departure of the low energy end of the high intensity integrated electron spectra (fig. 4.3) from the plateau shape of fig. 2.2, since retarded electrons could possess any energy below that of the threshold shoulder. Break-down of the high intensity limit assumption (II.6) for the lower intensity spectra causes a similar effect. Electrons produced near the pulse peak may experience a lesser field gradient later in the pulse if they are not accelerated from the focal region immediately. Any increase in the focal diameter is also important in determining the high intensity limit (equation 2.44), and can raise the intensity above which it is valid (to $\sim 10^{14} \text{ W cm}^{-2}$ for $d = 40 \mu\text{m}$ for example). This also affects the sharpness of the fall-off in the shoulder, since for peak

intensities greater than the threshold intensity, greater acceleration of the electrons (which are ionized early in the pulse) is possible if they are not immediately accelerated from the beam.

Further obscuring of the ionization threshold intensities on the integrated electron spectra may be due to the ill-defined nature of the threshold itself. It was assumed that outside the threshold intensity contour no ionization occurred but for ArII for example the ionization probability falls to 0.5 for an 8% decrease in intensity from threshold. For higher states the decrease required is less ($\sim 7\%$ for ArVI) but significant numbers of electrons may still be produced outside the ionized region. Variation in the pulse duration (11.5) also makes the threshold less well defined. The result is that electrons ionized outside the threshold intensity contour have less energy (and are more likely to be subject to coupling and delayed acceleration) and this causes a rounding of the characteristic shoulder threshold.

Finally, it must be noted that in all the analysis so far the single particle viewpoint has been taken. It is possible that for a significant ionized volume, collective plasma effects may be taking place, requiring the solution of coupled differential equations to determine the behaviour of the electrons as they are accelerated from the complex focal region. While evaluation of collective plasma effects is beyond the scope of the present work, some feeling for their significance can be seen in the number of particles N per Debye sphere (Holt and Haskell, 1965).

Using an electron energy defect of $\xi_{KIN} \sim 0.1 - 1$ eV on ionization

$$N = 9.4 \times 10^8 \xi_{KIN}^{3/2} n^{-1/2} \dots\dots\dots 4.1$$

$$\sim 20 - 500$$

which is large enough to suspect that such effects could be important.

CHAPTER V

CONCLUSION

The results of this experiment indicate that the electron energy spectra technique for the determination of threshold ionization intensities is limited fundamentally by shortcomings of the method itself, and also in this case by the large experimental errors. The former limitations are mainly due to electron-ion coupling, slow removal of electrons in comparison with the pulse duration, inadequate knowledge of focal volume characteristics and the presence of a significant partially ionized volume outside the threshold ionization contour. Variations in the pulse duration and the presence of impurities play a less important role and the limitation of collective plasma effects on this technique is not known.

Despite this it is possible from the results to discern at least three apparent ionization thresholds and this is corroborated by the agreement of the two semi-independent analyses used. The states observed were ArI, ArII and ArIV, and their position on the plot of ionization threshold intensity versus ionization potential in fig. 4.5 is fixed by the results of Boreham (1979c) which place the HeI and HeII states between them. Similarly, Boreham's result for HeII places a lower limit on the tentative observation of ArV. While these results must be treated with caution (as reflected by the large error bars used), the overall agreement with the Keldysh tunnelling model is evident and is not altered materially even if the ArV result corresponds to another state or is ignored altogether. The results for HeII, ArIV and ArV show a clear departure from the Raizer (multiphoton) approximation in the region where this process would not be expected to occur ($\gamma \sim 0.3 - 0.2$). In the region of overlap of the two predicted threshold plots the results for HeI and ArII provide confirmation, while ArI appears (despite the error bars) to lie between the two predicted results in the transition region $\gamma \sim 1$. Other calculations (table 2.1) indicate possibly an even lower predicted ArI tunnelling threshold than the $10^{14} \text{ W cm}^{-2}$ estimate shown in fig. 4.5. Neither the upper nor the lower ArI error bars for either technique quite reach the predicted ionization thresholds of the two limiting cases, and it was ArI that provided the most convincing and precise ionization threshold result. This experiment thus provides some indication of the validity of the Keldysh theory in the regime $\gamma \leq 1$.

In addition, the experiment gives further corroboration of the ponderomotive force model through the agreement between the two methods of estimating the threshold ionization intensities. High energy (up to 2 keV) electrons were again observed and the maximum energies produced were again found to be proportional to the intensity in agreement with equation 2.42.

Further improvements of this technique are limited by the fundamental difficulties above, although it is possible with better detection and intensity measuring equipment that greater definition may be possible to allow such closely spaced ionization states to be observed. The use of CO₂ lasers has been advocated by a number of writers (for example Delone, 1975) since its lower frequency enables investigation of ionization processes well into the tunnelling regime ($\gamma \propto \omega \ll 1$). The low CO₂ laser frequency takes on further significance in this technique since the ponderomotive force (equation 2.23) is inversely proportional to the square of the laser frequency. Greater electron energies may thus be obtained, increasing the electron velocity $V \propto \omega^{-1}$ by a factor of 10 in the high intensity limit. However, the larger wavelength also increases the focal diameter d , although possibly not by as much as 10. The overall decrease in the factor ωd would cause a decrease in the intensity defining the high intensity limit ($\propto (\omega d)^2$) thus ensuring more instantaneous acceleration of the ionized electrons. A similar effect results in a decrease in the strength of electron-ion coupling. However, the ionization probability is essentially frequency independent since tunnelling is not affected by the number of quanta (the electron is ionized in a short time compared to ω^{-1}), but it is strongly dependent on the field strength. Hence the difficulty of a significant partially ionized volume remains although it is possible that removal of the other limitations may sufficiently improve the feasibility of this technique.

It would be useful in any case to repeat the experiments in helium and argon using a CO₂ laser to verify the frequency independence of the ionization thresholds readily observed (He I, II and Ar I, II, IV) and to test for any variation in the lower states' ionization thresholds. The latter would investigate the effect of the transition region ($\gamma \sim 1$ for Nd and 0.1 for CO₂ for these states) on the tunnelling ionization probability. Also of interest would be the study of states with higher ionization potentials (and hence lower γ), particularly if well separated from the lower states. Lithium vapour is one such substance which, due to its univalent nature, has ionization states at 5.4 eV, 75.6 eV and 122.4 eV (Weast, 1974). These are accessible with present laser technology, the latter two states requiring threshold intensities of $9 \times 10^{15} \text{ W cm}^{-2}$ and $4 \times 10^{16} \text{ W cm}^{-2}$ from computer code calculations. Higher potential ionization states may exhibit departure from predicted thresholds once intensities of $10^{17} \text{ W cm}^{-2}$ are exceeded and the oscillation energy of the electron causes it to become relativistic. Theoretical extension of the Keldysh theory to allow for relativistic velocities in the final state could provide predicted ionization thresholds for experimental comparison. While this would require higher power lasers than are at present available, it would permit investigation of inner shell ionization states whose large separation from the outer shell could well be resolved by the electron spectra technique.

REFERENCES

- Agostini, P., Barjot, G., Bonnal, J.F., Mainfray, G., Manus, C. and Morellec, J. — 1968. *IEEE J. Quant. Electron.* **4**, 667.
- Agostini, P., Barjot, G., Mainfray, G., Manus, C. and Thebault, J. — 1970. *IEEE J. Quant. Electron.* **6**, 782.
- Alimov, D.T. and Delone, N.B. — 1976. *Sov. Phys. JETP.* **43**, 15.
- Arslanbekov, T.U., Delone, N.B., Masalov, A.V., Todirashku, S.S., Fainshtein, A.G. — 1977. *Sov. Phys. JETP.* **45**, 473.
- Bakos, J.S. — 1974. *Advan. Electron. Electron Phys.* **36**, 57.
- Boreham, B.W. — 1979a. 12th AINSE Plasma Physics Conference, Lucas Heights, N.S.W., Australia, February.
- Boreham, B.W. — 1979b. Laser Physics Group Tech. Report, No. 9
- Boreham, B.W. — 1979c. Europhysics Study Conference on Multiphoton Processes, Benodet, France, June 18–22.
- Boreham, B.W. and Hora, H. — 1979. *Phys. Rev. Lett.* **42**, 776.
- Boreham, B.W. and Hughes, J.L. — 1978a. *Search*, **9**, 328.
- Boreham, B.W. and Hughes, J.L. — 1978b. Proceedings of the 10th International Quantum Electronics Conference, Atlanta, Ga., U.S.A., May 29 — June 1, J.O.S.A. **68**, 698.
- Boreham, B.W., Luther-Davies, B. and Hughes, J.L. — 1978. IX National Conference on Coherent and Non-Linear Optics, Leningrad, June 13–16.
- Boreham, B.W. and Luther-Davies, B. — 1979. *Journal of Applied Physics* (to be published).
- Boreham, B.W. and Mavaddat, R. — 1978. IX International Conference on Coherent and Non-Linear Optics, Leningrad, June 13–16.
- Boreham, B.W., Mavaddat, R., Hughes, J.L. and Hora, H. — 1978. 11th International Symposium on Rarefied Gas Dynamics, Cannes, France, July 3–8.
- Bradley, D.J. and New, G.H.C. — 1974. *Proc. IEEE.* **62**, 313.
- Chen, F.F. — 1974a. *Introduction to Plasma Physics*. (Plenum Press).
- Chen, F.F. — 1974b. *Laser Interaction and Related Plasma Phenomenon*, Vol. 3A, (Plenum Press), 291.
- Chin, S.L. and Isenor, N.R. — 1970. *Can. J. Physics.* **48**, 1445.
- Choudhury, B.J. — 1973a. *J. Phys. B: Atom. Molec. Phys.* **6**, L100.
- Choudhury, B.J. — 1973b. *J. Phys. B: Atom. Molec. Phys.* **6**, L103.

- Delacroix, J.L. — 1965. *Plasma Physics*. (Wiley).
- Del Pizzo, V. — 1979. Ph.D. Thesis, Australian National University.
- Delone, G.A. and Delone, N.B. — 1969. *Sov. Phys. JETP Lett.* **10**, 265.
- Delone, N.B. — 1975. *Sov. Phys. Usp.* **18**, 169.
- Drummond, J.E. — 1961. *Plasma Physics*. (McGraw-Hill).
- Gold, A. and Bebb, H.B. — 1965. *Phys. Rev. Lett.* **14**, 60.
- Gontier, Y., Rahman, N.K. and Trahin, M. — 1975. *Phys. Rev. Lett.* **34**, 779.
- Gontier, Y. and Trahin, M. — 1978. *J. Phys. B: Atom. Molec. Phys.* **11**, L441.
- Grey-Morgan, C. — 1975. *Rep. Prog. Phys.* **38**, 621.
- Guyot, A., Bettinger A. and Auric, D. — 1978. *Rev. de Phys. App.* **13**, 198.
- Hollis, M.J. — 1976. Laser Group Technical Report No. 1.
- Hollis, M.J. — 1978. *Optics Communications*, **25**, 395.
- Holt, E.M. and Haskell, R.E. — 1965. *Foundations of Plasma Dynamics*. (MacMillan).
- Hora, H. — 1969a. *Z. Physik.* **226**, 156.
- Hora, H. — 1969b. *Physics of Fluids.* **12**, 182.
- Hora, H. — 1971. *Laser Interaction and Related Plasma Phenomena*. Vol. 1, (Plenum Press), 383.
- Hora, H. — 1972. *Laser Interaction and Related Plasma Phenomena*. Vol. 2, (Plenum Press), 341.
- Hora, H. — 1975. *Laser Plasmas and Nuclear Energy*. (Plenum Press).
- Hora, H. — 1977. *Laser Interaction and Related Plasma Phenomena*. Vol. 4B, (Plenum Press), 841.
- Hora, H., Kane, E.L. and Hughes, J.L. — 1978. *J. Appl. Phys.* **49**, 923.
- Hughes, T.P. — 1975. *Plasma and Laser Light*. (Adam-Hilger).
- Kazantsev, A.P. — 1978. *Sov. Phys. Usp.* **21**, 58.
- Keen, B.E. — 1974. Editor, *Plasma Physics*. (Institute of Physics London and Bristol).
- Keldysh, L.V. — 1965. *Sov. Phys. JETP.* **20**, 1307.
- Kelly, R.L. and Harrison, D.E. Jr. — 1971. *Atomic Data.* **3**, 177.
- Koechner, W. — 1976. *Solid State Laser Engineering*. (Springer-Verlag).

- Lambropoulos, P. — 1976. *Advances in Atomic and Molecular Physics*. Vol. 12, Ed. D.R. Bates and B. Bederson. (New York: Academic Press), 86.
- Landau, L.D. and Lifshitz, E.M. — 1960. *Electrodynamics of Continuous Media*. (Pergamon Press).
- Lecompte, C., Mainfray, G., Manus, C. and Sanchez, F. — 1974. *Phys. Rev. Lett.* **32**, 265.
- Lecompte, C., Mainfray, G., Manus, C. and Sanchez, F. — 1975. *Phys. Rev. A*. **11**, 1009.
- Lompre, L.A., Mainfray, G., Manus, C., Repaux, S. and Thebault, J. — 1976. *Phys. Rev. Lett.* **36**, 949.
- Lompre, L.A., Mainfray, G., Manus, C. and Thebault, J. — 1977. *Phys. Rev. A*. **15**, 1604.
- Lompre, L.A., Mainfray, G., Manus, C. and Thebault, J. — 1978. *J. de Phys.* **39**, 610.
- Lorrain, P. and Corson, D.R. — 1970. *Electromagnetic Fields and Waves*. (W.H. Freeman and Co.).
- Luther-Davies, B., Boreham, B.W., Hughes, J.L. and Hollis, M.J. — 1978. Proceedings of the 10th International Quantum Electronics Conference, Atlanta, Ga., U.S.A. May 29 — June 1, *J.O.S.A.* **68**, 658.
- Luther-Davies, B. — 1977. *Optics Communications*, **23**, 98.
- Luther-Davies, B. and Hughes, J.L. — 1976. *Optics Communications*, **18**, 351.
- Mandel, L. and Wolfe, E. — 1965. *Rev. Mod. Phys.* **37**, 241.
- Martin, E.A. and Mandel, L. — 1976. *Applied Optics*, **15**, 2378.
- Miyazaki, K. and Kashiwagi, H. — 1978. *Phys. Rev. A*. **18**, 635.
- McLean, W.A. and Swain, S. — 1978. *J. Phys. B: Atom. Molec. Phys.* **11**, L515.
- Mohan, M. — 1973. *J. Phys. B: Atom. Molec. Phys.* **6**, 1218.
- Morellec, J., Normand, D. and Petite, G. — 1976. *Phys. Rev. A*. **14**, 300.
- Perelemov, A.M., Popov, V.S. and Terentev, M.V. — 1966. *Sov. Phys. JETP*. **23**, 924.
- Peressini, E.R. — 1966. *Physics of Quantum Electronics*. Ed. P.L. Kelly, B. Lax and P.E. Tannenwald. N.Y. (McGraw-Hill). 499.
- Nikishov, A. and Ritus, V.I. — 1967. *Sov. Phys. JETP*. **25**, 145.
- Raizer, Y.P. — 1966. *Sov. Phys. USPEKHI*. **8**, 650.
- Reiss, H.R. — 1970. *Phys. Rev. Lett.* **25**, 1149.
- Rosenberg, L. — 1978. *Phys. Rev. A*. **18**, 2557.
- Spitzer, L. Jr. — 1962. *Physics of Fully Ionized Gases*. 2nd ed.) (Wiley).

Stenholm, S. -- 1979. *Contemp. Phys.* **20**, 37.

Uman, M.A. -- 1964. *Introduction to Plasma Physics.* (McGraw-Hill).

Voronov, G.S. -- 1966. *Sov. Phys. JETP*, **51**, 1009

Voronov, G.S., Delone, G.A. and Delone, N.B. -- 1966. *Sov. Phys. JETP Lett.* **3**, 313.

Weast, R.C. -- 1974. *Handbook of Chemistry and Physics.* (Chemical Rubber Co.).